This Accepted Manuscript has not been copyedited and formatted. The final version may differ from this version. A link to any extended data will be provided when the final version is posted online.

JNeurosci
THE JOURNAL OF NEUROSCIENCE

JNeurosci Accepted Manuscript

Research Articles: Development/Plasticity/Repair

N-cadherin orchestrates self-organization of neurons within a columnar unit in the *Drosophila* medulla

Olena Trush[1], Chuyan Liu[1], Xujun Han[2], Yasuhiro Nakai[2], Rie Takayama[2], Hideki Murakawa[3], Jose A. Carrillo[4], Hiroki Takechi[5], Satoko Hakeda-Suzuki[5], Takashi Suzuki[5] and Makoto Sato[1,2]

[1]*Laboratory of Developmental Neurobiology, Graduate School of Medical Sciences*

[2]*Mathematical Neuroscience Unit, Institute for Frontier Science Initiative, Kanazawa University, 13-1 Takaramachi, Kanazawa, Ishikawa 920-8640, Japan*

[3]*Faculty of Science and Technology, Ryukoku University, 1-5 Yokotani, Seta Oe-cho, Otsu, Shiga 520-2194, Japan. 1-5 Yokotani, Seta Oe-cho, Otsu, Shiga 520-2194, Japan*

[4]*Department of Mathematics, Imperial College London, South Kensington Campus, London SW7 2AZ, UK*

[5]*School of Life Science & Technology, Tokyo Institute of Technology, Yokohama, Kanagawa 226-8501, Japan.*

https://doi.org/10.1523/JNEUROSCI.3107-18.2019

Received: 11 December 2018

Revised: 9 May 2019

Accepted: 15 May 2019

Published: 7 June 2019

Author contributions: O.T., H.M., J.A.C., and M.S. designed research; O.T., C.L., X.H., R.T., H.M., and M.S. performed research; O.T., H.M., and M.S. analyzed data; O.T. wrote the first draft of the paper; O.T. and M.S. edited the paper; O.T., H.M., J.A.C., and M.S. wrote the paper; C.L., X.H., Y.N., H.T., S.H.-S., and T.S. contributed unpublished reagents/analytic tools.

Conflict of Interest: The authors declare no competing financial interests.

We thank Hugo Bellen, Takashi Hayashi, Aljosha Nern, Takumi Suzuki and Tetsuo Yasugi for critical comments on the manuscript. We are grateful to Martin Heisenberg, Graeme Mardon, Hideji Murakoshi, Tadashi Uemura and S. Lawrence Zipursky for reagents and fly strains. We thank Bloomington Stock Center, Vienna ***Drosophila*** RNAi Center and DGRC, Kyoto for fly strains and Developmental Study Hybridoma Bank (DSHB) for antibodies. This work was supported by Grant-in-Aid for JSPS Research Fellow (to O.T.), CREST from JST, Grant-in-Aid for Scientific Research (B) from MEXT, Takeda Science Foundation and Cooperative Research of 'Network Joint Research Center for Materials and Devices' (to M.S.), and by Grant-in-Aid for Scientific Research on Innovative Areas from MEXT (To M.S. and T.S.).

Correspondence: makotos@staff.kanazawa-u.ac.jp

Cite as: J. Neurosci 2019; 10.1523/JNEUROSCI.3107-18.2019

Alerts: Sign up at www.jneurosci.org/alerts to receive customized email alerts when the fully formatted version of this article is published.

Accepted manuscripts are peer-reviewed but have not been through the copyediting, formatting, or proofreading process.

Copyright © 2019 the authors

JNeurosci Accepted Manuscript

N-cadherin orchestrates self-organization of neurons within a columnar unit in the *Drosophila* medulla

abbreviated title: N-cadherin regulates column formation in the fly medulla

Olena Trush[1,6], Chuyan Liu[1,6], Xujun Han[2], Yasuhiro Nakai[2], Rie Takayama[2], Hideki Murakawa[3], Jose A. Carrillo[4], Hiroki Takechi[5], Satoko Hakeda-Suzuki[5], Takashi Suzuki[5] and Makoto Sato[1,2,*]

[1]Laboratory of Developmental Neurobiology, Graduate School of Medical Sciences, [2]Mathematical Neuroscience Unit, Institute for Frontier Science Initiative, Kanazawa University, 13-1 Takaramachi, Kanazawa, Ishikawa 920-8640, Japan, [3]Faculty of Science and Technology, Ryukoku University, 1-5 Yokotani, Seta Oe-cho, Otsu, Shiga 520-2194, Japan. 1-5 Yokotani, Seta Oe-cho, Otsu, Shiga 520-2194, Japan, [4]Department of Mathematics, Imperial College London, South Kensington Campus, London SW7 2AZ, UK, [5]School of Life Science & Technology, Tokyo Institute of Technology, Yokohama, Kanagawa 226-8501, Japan. [6]These authors contributed equally to this work.

*Correspondence: makotos@staff.kanazawa-u.ac.jp

The number of pages: 64

The number of figures: 10

The number of tables: 0

The number of multimedia: 5

JNeurosci Accepted Manuscript

19 The number of 3D models: 0

20 The number of words for Abstract: 150

21 The number of words for Introduction: 645

22 The number of words for Discussion: 1500

23

24 **Conflict of interests**

25 No potential **conflicts of interest** were disclosed.

26

27 **Acknowledgments**

28 We thank Hugo Bellen, Takashi Hayashi, Aljosha Nern, Takumi Suzuki and Tetsuo Yasugi for critical
29 comments on the manuscript. We are grateful to Martin Heisenberg, Graeme Mardon, Hideji Murakoshi,
30 Tadashi Uemura and S. Lawrence Zipursky for reagents and fly strains. We thank Bloomington Stock
31 Center, Vienna *Drosophila* RNAi Center and DGRC, Kyoto for fly strains and Developmental Study
32 Hybridoma Bank (DSHB) for antibodies. This work was supported by Grant-in-Aid for JSPS Research
33 Fellow (to O.T.), CREST from JST, Grant-in-Aid for Scientific Research (B) from MEXT, Takeda
34 Science Foundation and Cooperative Research of 'Network Joint Research Center for Materials and
35 Devices' (to M.S.), and by Grant-in-Aid for Scientific Research on Innovative Areas from MEXT (To
36 M.S. and T.S.).

JNeurosci Accepted Manuscript

37

JNeurosci Accepted Manuscript

Abstract

Columnar structure is a basic unit of the brain, but the mechanism underlying its development remains largely unknown. The medulla, the largest ganglion of the *Drosophila melanogaster* visual center, provides a unique opportunity to reveal the mechanisms of three-dimensional organization of the columns. In this study, using N-cadherin (Ncad) as a marker, we reveal the donut-like columnar structures along the two-dimensional layer in the larval medulla that evolves to form three distinct layers in pupal development. Column formation is initiated by three core neurons, R8, R7, and Mi1, which establish distinct concentric domains within a column. We demonstrate that Ncad-dependent relative adhesiveness of the core columnar neurons regulates their relative location within a column along a two-dimensional layer in the larval medulla according to the differential adhesion hypothesis. We also propose the presence of mutual interactions among the three layers during formation of the three-dimensional structures of the medulla columns.

Significance statement

The columnar structure is a basic unit of the brain, but its developmental mechanism remains unknown. The medulla, the largest ganglion of the fly visual center, provides a unique opportunity to reveal the mechanisms of three-dimensional organization of the columns. We reveal that column formation is initiated by three core neurons that establish distinct concentric domains within a column. We

JNeurosci Accepted Manuscript

demonstrate the *in vivo* evidence of N-cadherin-dependent differential adhesion among the core columnar neurons within a column along a two-dimensional layer in the larval medulla. The two-dimensional larval columns evolve to form three distinct layers in the pupal medulla. We propose the presence of mutual interactions among the three layers during formation of the three-dimensional structures of the medulla columns.

Introduction

The columnar unit is a basic feature of the brain. In the cerebral cortex, microcolumns are cell-type–specific radial clusters of neurons that are found in nearly all examined cortical regions (Mountcastle, 1997; Maruoka et al., 2017). However, the developmental mechanisms underlying columnar unit formation remain unclear.

The fly visual center, which receives visual input from the eye, shares structural characteristics with the mammalian cerebral cortex, such as the columnar and layered structures (Sanes and Zipursky, 2010). The retina is the compound eye consisting of 800 ommatidial units, and each ommatidium contains eight photoreceptor neurons, R1-8. Visual information received in the retina is transmitted to the optic lobe in the brain (Sato et al., 2013; Zhu, 2013; Neriec and Desplan, 2016). R1-6 project to the first optic ganglion, the lamina, where lamina neurons L1-5 form a columnar unit called a cartridge. R7, R8, and L1-5 then project to the second optic ganglion, the medulla, where as many as 100 neurons form a

JNeurosci Accepted Manuscript

columnar unit. Some of these neurons project through the medulla to the third optic ganglion, the lobula and lobula plate. In comparison with the simple structures of ommatidia in the retina and cartridges in the lamina, columns in the medulla show complex three-dimensional structures that are analogous to the microcolumns in the mammalian cerebral cortex (Fig. 1A) (Takemura et al., 2013). Indeed, the developmental mechanisms underlying microcolumns and medulla columns share similarities. A single neuroblast (NB), a neural stem-like cell, produces a group of radially oriented and clonally related neurons in the developing medulla (Fig. 1A)(Hasegawa et al., 2011; Morante et al., 2011), which is analogous to the radial unit produced from a single neural stem cell and migrates along the same radial fiber in the developing cerebral cortex (Rakic, 1988; Mountcastle, 1997; Noctor et al., 2004; Li et al., 2012; Ohtsuki et al., 2012). These characteristics of the medulla, together with the powerful techniques available in fly genetics, make it an excellent model for studying column formation.

In this study, we show that the cell adhesion molecule N-cadherin (Ncad) (Iwai et al., 1997) and F-actin binding molecule phalloidin reveal a donut-like structure of the medulla column. The two-dimensional donut-like pattern in the larval medulla evolves to establish the three-dimensional pattern in the top, middle, and bottom layers during pupal development. We identified three core columnar neurons essential for column formation in larval development. The terminal of R7 occupies the dot-like central region of the larval column. The R8 terminal enwraps the R7 terminal forming a donut-like region that overlaps with the Ncad/phalloidin pattern. The Mi1 terminal occupies a grid-like

JNeurosci Accepted Manuscript

region outside the R8 terminal. Thus, R7, R8, and Mi1 form the two-dimensional concentric organization composing the three distinct domains in the larval medulla.

Ncad is expressed in R7, R8, L1-5, and Mi1 neurons (Lee et al., 2001; Ting et al., 2005; Yonekura et al., 2007; Nern et al., 2008; Petrovic and Hummel, 2008; Hasegawa et al., 2013). Ncad-dependent cell adhesion among these neurons may regulate column formation. The differential adhesion hypothesis (DAH) proposes that mixtures of cell populations segregate according to their adhesive properties: the less-adhesive cell population is located at the periphery of the cell aggregates and surrounds the more-adhesive cells (Steinberg and Takeichi, 1994; Murakawa and Togashi, 2015). Roles of Ncad-dependent differential adhesion have been proposed in lamina cartridge formation (Iwai et al., 2002; Schwabe et al., 2014). In this study, we establish a series of genetic tools that can specifically express fluorescent markers and manipulate Ncad activity in R7, R8, and Mi1 in the medulla. By using these tools, we clearly demonstrate the *in vivo* evidence of DAH among R7, R8, and Mi1 in the medulla column formation. Additionally, by using a mathematical model based on the differential adhesiveness of these neurons, we also demonstrate that differential adhesion could be the major driving force in establishing the columnar structure.

Materials and methods

JNeurosci Accepted Manuscript

Fly strains

Fly strains were maintained on standard *Drosophila* medium at 25°C. For all experiments in this study, both male and female flies were used. Following fly strains were used: *sens^{E2} FRT 80B* (Frankfort et al., 2001), *sev*^{14} (BDSC5689), *bsh*^{1}, *bsh*^{2} (Hasegawa et al., 2013), *Ncad ^{M19}FRT40A* (Iwai et al., 1997), *sensF2-Gal4* (Atkins et al., 2013), *sevPM181-Gal4* (Lee et al., 2001), *R69B02-Gal4* (L1-5; BDSC39478), *c202-Gal4* (L1) (Rister et al., 2007), *R16H03-Gal4* (L2; BDSC48744), *R20A03-Gal4* (L3; BDSC48871), *R31C06-Gal4* (L4; BL49883), *R13E12-Gal4* (Tm3; BDSC48569), *R42F06-Gal4* (T4-5; BDSC41253), *drf-Gal4* (Hasegawa et al., 2011), *GMR-FRT-stop-FRT-Gal4* (Chen et al., 2014), *arm-lacZ FRT80B* (BDSC6341), *sens-FLPG5* (R8; BDSC55768), *20C11-FLPG5* (R7; *R27G05G5.PEST-FLP* (L1-5; *R27G05-FLPG5* (L1-5; BDSC55765), *UAS-bshRNAi* (VDRC106634), *UAS-NcadRNAi* (BDSC27503, VDRC1092), *UAS-sevRNAi* (BDSC55866), *UAS-rpr* (BDSC5824), *UAS-Ncad$^{7a, 13a, 18a}$* (Iwai et al., 1997), *hs-flp*, *tub-Gal80 FRT40A*, *tub-Gal80 FRTG13*, *y^{+} FRT40A*. Following fly strains were generated in this work: *bshM-Gal4*, *bshL-Gal4*, *UAS-myrGFP*, *UAS>Gal80>myrGFP*, *R27G05-LexA* (L1-5), *sevEnS-LexA*, *sensF2-LexA*, *bshM-LexA*, *LexAop-myrTomato*, *Ncad-FsF-GFP*, *hth-FLP*.

Generation of Gal4 and LexA strains

pGEattB-bshSPGal4 vector was generated by inserting *bsh* short promoter (*bshSP*) and *Gal4 (IVS-Syn21-Gal4-p10)*(Pfeiffer et al., 2012) fragments into *pGEattB* vector (Huang et al., 2009).

JNeurosci Accepted Manuscript

Lamina-specific *bshL-Gal4* and medulla-specific *bshM-Gal4* were generated by inserting *bshD* fragment together with *bshPA* and *bshPB* fragments into *pGEattB-bshSPGal4*, respectively. *pGEattB-LexA* vector was generated by inserting *LexA* (*LHV2*)(Yagi et al., 2010). fragment into *pGEattB*. Medulla-specific *bshM-LexA* was generated by inserting *bshD*, *bshPB* and *bshSP* fragments into *pGEattB-LexA*. *sevEnS-LexA* construct was generated by inserting *sev* enhancer (*sevEnS*) and *sev* promotor (*sevPro*) fragments into *pGEattB-LexA*. *sensF2-LexA* was generated by inserting *sens* enhancer (*sensF2*) and *sens* promoter (*sensPro*) fragments into *pGEattB-LexA. R27G05-LexA* was generated by inserting *R27G05* and *hsp70* promoter fragment into *pGEattB-LexA*. *bshSP* (1.4kb), *bshD* (2.0kb), *bshPA* (552bp), *bshPB* (378bp), *sevEnS* (1.3kb), *sevPro* (1kb), *sensF2* (650bp), and *sensPro* (1.5kb) fragments were amplified using the following PCR primers: *bshSP* (ACTAGTTAACACAAACCCCATAACCCCC and GTAGCTTCATGGATCCCATTGCCATTGCGCTGGAGGATG), *bshD* (TATAGATCTGCGGCCGCGTTAGGTTGTTAACCTAAGC and CTGTTTAAGGGAATTCGCCGCTATTGAAGATTACCCAG), *bshPA* (GAATTCCCTTAAACAGGAACTACAAGTACG and GTTTGTGTTAACTAGTGCCTAATTTCCCATTGTTGC), *bshPB* (GAATTCCCTTAAACAGGAACTACAAGTACG and GTTTGTGTTAACTAGTGAGCTCCATAGAAGTGGAAAGC), *sevEnS* (TTCTTGCATGCAATGCGGCCGCTTATTAGCGAGATGCTCGAGGTCTCTC and

JNeurosci Accepted Manuscript

TTGGTCTGCAGTTGAGTATCCTGGTCTTCCTGCTCGAGATCC) and *sevPro* (CACTCAACTGCAGACCAATTCTGATTGTGTGGGCTAGTTCCC and TTAACGCTTTCATGGCGCGCCTATCTGGATCTGGATGTGCGATTCCCG), *sensF2* (AATTCTTGCATGCAATGCGGCCGCGTGGAAAAGTGGCACAGCAAATACTGTCATA and TATCTGAAGCTAGCAACTCGGAAGTTGGCAAAGCTCGAAAGG) and *sensPro* (GAGTTGCTAGCTTCAGATACGAGAAGATGGGGACTTTATGGCT and CGTTAACGCTTTCATGGCGCGCCGATTCGAACGGATCTTCGATGGGTC).

Generation of *UAS>Gal80>myrGFP*, *UAS-myrGFP* and *LexAop-myrTomato* strains

UAS>Gal80>myrGFP was generated by inserting *hsp70 promoter-FRT*, *Syn21-Gal80*, *STOP-FRT-IVS* and *Syn21-myr::GFP* into *pJFRC164* (addgene; (Pfeiffer et al., 2012), and was co-injected with *PhiC31* integrase into the *VK00005 attP* landing site. *FRT-Gal80-FRT* cassette was permanently removed using *FLPase* to generate *UAS-myrGFP* fly strain. *LexAop-myrTomato* was generated by inserting *Syn21-myr::Tomato* fragment from *HM29-37 MCS-tdTomato/pCPCI3* (gift from Hideji Murakoshi) into *pJFRC19* and was co-injected with *PhiC31* integrase into the *ZH-22A attP* landing site. *hsp70 promoter-FRT*, *Syn21-Gal80*, *STOP-FRT-IVS*, *Syn21-myr::GFP* and *Syn21-myr::Tomato* fragments were amplified using the following PCR primers: *hsp70 promoter-FRT* (ACTCTAGCGCTAGCGACGTCG and TTTTTTTTTTAAGTTCTAGCTAGCTTACGTTAGAAG), *Syn21-Gal80*

JNeurosci Accepted Manuscript

(AACTTAAAAAAAAAAATCAAAATGGACTACAACAAGAG and

TTGGCTTTAGTCGACTTAACCGGTTTATAAACTATAATGC), *STOP-FRT-IVS*

(GTCGACTAAAGCCAAATAGA and CCTCGAGCCGCGGCCGCCTGA), *Syn21-myr::GFP*

(catGGTACCAACTTAAAAAAAAAAATCAAAATGGGCAACAAATGCTGCAG and

TTACTTGTAGAGCTCATCCATG) and *Syn21-myr::Tomato*

(CGGCCGCGGCTCGAGGGTACCAACTTAAAAAAAAAAATCAAAATGGGCAACAAATGCTGC

AG and ACGATTCATTTAAGGCCTTTACTTGTACAGCTCGTCC).

Generation of *hth-FLP* strain

The 3rd exon of endogenous *hth* was replaced by the fragment containing *attP* via the homologous recombination with the homology arms for *hth* (*hthLp* and *hthRp*; Huang et al., 2009). The *hthKnockinFLP-p10* vector was generated by inserting a short bridge fragment containing a part of the 2nd intron and 3rd exon of *hth* (*hth_inEx*), *FLP* and *p10* into *pGEattB* vector. *hthLp* (1.8kb) and *hthRp* (2.0kb), *hth_inEx*, *FLP* and *p10* fragments were amplified using the following PCR primers: *hthLp*

(CATGCGGCCGCCCAAGTGACCCGAGATGATCTT and

CATGGTACCTGGATTGCCTCAAAAACCCAGG), *hthRp*

(CATGGCGCGCCCAGGTAAGAATAATGGCCCCAG and

CATCTCGAGCCTTAGCTGCATCATTAGCAGC), *hth_inEx*

JNeurosci Accepted Manuscript

(CATCATGCGGCCGCCCTGGGTTTTTGAGGCAATCCA and CATGGCGCGCCGGAATAGCGGATGTCTGCAATGG), *FLP* (CGCTATTCCGGCGCGCCATGCCACAATTTGATATATTATG and GCTAGCTTATATGCGTCTATTTATGTAG) and *p10* (CGCATATAAGCTAGCATGAATCGTTTTTAAAATAAC and TTATACGAAGTTATGGTACCTCGAATCGCTATCCAAGCCAG). The *hthKnockinFLP-p10* was co-injected with PhiC31 integrase into the *attP* site in the *hth* locus.

Generation of Ncad-FsF-GFP knock-in allele

Ncad-FsF-GFP knock-in allele was generated by CRISPR/Cas9 technology (Kondo and Ueda, 2013). A knock-in vector containing the homology arms for Ncad (*NcadL* and *NcadR*), the flip-out cassette with *GFP* (*FRT-stop-FRT-GFP*) and the red fluorescent transformation marker gene (*3xP3RFP*) was generated by ligating *NcadL* (555bp), *FRT*, *stop-FRT*, *GFP*, *3xP3RFP* and *NcadR* (518bp) fragments amplified using the following PCR primers: *NcadL* (TATAGAGCTCACCCATTATGCAGCCGTTTAGTC and TATAGCGGCCGCACAATTCTAGTTCGGTATTGTGGGG), *NcadR* (TATACTCGAGGCTGGTGGAGCGAGCAGTGA and TATAGGTACCGCGCTCCTAAACTAAACTTTGGTATGC), *FRT*

JNeurosci Accepted Manuscript

(TATAGCGGCCGCATTGAAGTTCCTATTCCGAAGTTCC and

TATAACTAGTCAAAAGCGCTCTGAAGTTCCTATAC), *stop-FRT*

(TATAACTAGTTAAATCCAGACATGATAAGATACATTGATGAG and

TATACTGCAGCAAAAGCGCTCTGAAGTTCCTATAC), *GFP*

(TATACTGCAGATGAGTAAAGGAGAAGAACTTTTC and

TATACTCGAGTCTAGTGGATCCAGACATGATAAG), *3xP3RFP*

(GCGCCTCGAGAACTTCGTATAGCATACATTA and

TATACTCGAGAACGTGTCGGTACCAATTGAGCTC). A gRNA vector (*pBFv-U6.2*) that recognize the sequences containing the stop codon of *Ncad* gene (GAACTAGAATTG**TAA**GCTGGTGG), was injected to eggs carrying *vas-Cas9* (BDSC 55821) together with the knock-in vector. The precise integration of the knock-in vector was verified by PCR and sequencing. The *3xP3RFP* flanked by two *loxP* sites was removed by the heat induction of *Cre*. We also generated *Ncad-GFP* allele by permanently removing the *FsF* cassette from *Ncad-FsF-GFP* using FLPase. The *Ncad-GFP* patterns were indistinguishable from the Ncad antibody patterns, suggesting that the *Ncad-FsF-GFP* allele reliably recapitulates Ncad protein distribution.

Histochemistry

JNeurosci Accepted Manuscript

Immunohistochemistry was performed as described before (Hasegawa et al., 2011)). The following primary antibodies were used: rat anti-Ncad (1:20, DSHB), mouse anti-Chaoptin (24B10, 1:20, DSHB), guinea pig anti-Bsh (1:500)(Hasegawa et al., 2011), mouse anti-LacZ (1:250, Promega), chicken anti-LacZ (1:2000, abcam). The secondary antibodies were used: anti-mouse Cy3, anti-mouse Cy5, anti-guinea pig Cy5, anti-guinea pig FITC, anti-rat Cy5, anti-chicken Cy3 (Jackson ImmunoResearch Laboratories). Phalloidin staining was performed by TRIC-Phalloidin (1:200, Sigma). Confocal images were obtained by Zeiss LSM 880 and a super-resolution unit Zeiss Airyscan. 40x 1.2NA water immersion and 63x 1.4NA oil immersion lenses were used for regular confocal and super-resolution imaging, respectively. The default Airyscan filtering mode (filter strength of 6.0) with the 3D reconstruction algorithm was used. Images were processed using Zeiss LSM image browser ZEN and Adobe Photoshop.

Quantification of Ncad expression level

To quantify the level of Ncad expression, the photon counting mode of LSM880 confocal microscopy was used. Ncad-FsF-GFP expressing axon terminals in the larval medulla were focused, and numbers of photons emitted from the terminals were quantified in each pixel area to compare the photon density for different neuron types. Sizes of the pixel area were categorized according to the number of photons

JNeurosci Accepted Manuscript

emitted. Background photons were counted outside the GFP labelled clones and were subtracted from the number of photons emitted from the axon terminals.

Experimental Design and Statistical Analysis

The experiments in Figs. 6-9 were designed and quantified as described below, and statistically tested by t-test. P values are indicated in the figure legends.

Quantification of columnar defects

Fiji was used to quantify the columnar defects (see Figs. 7 and 9). Phalloidin was used as a column marker. The outer and inner rings of phalloidin staining were manually outlined by the oval selection tool. Essentially the same results were obtained when Ncad was used as a marker. The total amount of GFP signal and the oval size were measured. Here, *o* and *i* indicate the total GFP amount within the outer and inner rings, respectively. *o-i* indicates the GFP amount within the Ncad+ ring region. The GFP amount was divided by the area size of interest to normalize the size effect. Relative GFP density between distinct domains of the column was calculated as follows. Expansion and redirection ratios of R7 are o/i and (*o-i*)/*i*, respectively (see Fig. 7). When we knock-down *Ncad* in R8, the entire growth cone of a single R8 was outlined by the oval selection tool to measure the total amount of GFP (*w*). Relative GFP amount between distinct domains of the column was calculated. Expansion and redirection ratios of R8

JNeurosci Accepted Manuscript

are *w/o* and (*w*-*o*)/*o*, respectively (see Fig. 7). When we overexpress *Ncad* in Mi1 and R8, expansion and redirection ratios are *o*/(*o*-*i*) and *i*/(*o*-*i*), respectively (see Fig. 9).

In Fig. 8, individual R7 or R8 terminals were manually outlined by the oval selection tool. The mean intensity of Tomato signal inside the selected area was normalized by the mean intensity of Tomato signal inside a wider area containing multiple columns to obtain expansion ratios of Mi1 or R8. A ROI of 100 x 70 was selected by the rectangle selection tool to crop an area in which both of GFP (R8) and Tomato (Mi1) signals are focused. Coloc 2 function of Fiji was used to calculate the Pearson's R value to quantify the colocalization between two neurons.

Mathematics and Equations

We model the neuronal cell segregation by modifying the continuous model of cell-cell adhesion (Murakawa and Togashi, 2015; Carrillo et al., 2019). The densities of the three cell types of neurons at position $\boldsymbol{x} \in \mathbb{R}^2$ and time $t \geq 0$ are denoted by $u = u(\boldsymbol{x}, t), v(\boldsymbol{x}, t), w = w(\boldsymbol{x}, t)$, respectively. Each of the equations in the system represents the evolution in time of the densities *u*, *v*, *w* under a velocity field containing volume exclusion effect and attractive forces. The nondimensional system reads as

JNeurosci Accepted Manuscript

$$\begin{cases} \dfrac{\partial u}{\partial t} = \nabla \cdot (u \nabla \sigma) - \nabla \cdot \big(u(1-\sigma)\boldsymbol{K}_1(u,v,w)\big) \\ \dfrac{\partial v}{\partial t} = \nabla \cdot (v \nabla \sigma) - \nabla \cdot \big(v(1-\sigma)\boldsymbol{K}_2(u,v,w)\big) \\ \dfrac{\partial w}{\partial t} = \nabla \cdot (w \nabla \sigma) - \nabla \cdot \big(w(1-\sigma)\boldsymbol{K}_3(u,v,w)\big) \end{cases}$$

where $\sigma = u + v + w$ is the total population of cells, and the interaction attractive kernels $\boldsymbol{K_i}$ ($i = 1$, 2, 3) are given by

$$\boldsymbol{K}_i(u,v,w)(\boldsymbol{x}) = \frac{1}{R}\int_0^R \int_{S^1} [a_{i1}u(\boldsymbol{x}+r\boldsymbol{\eta}) + a_{i2}v(\boldsymbol{x}+r\boldsymbol{\eta}) + a_{i3}w(\boldsymbol{x}+r\boldsymbol{\eta})]\,\omega(r)\,r\boldsymbol{\eta}\,d\boldsymbol{\eta}\,dr$$

Here, R is a positive constant called the sensing radius, that is rescaled to be one, S^1 is the unit circle, a_{ij} ($i, j = 1, 2, 3$) denote the adhesive strength parameters between the ith and jth species, and ω is a function describing how the adhesion force depends at a distance r from position x, which is defined $\omega \equiv 1$ here. The attractive forces model nonlocal adhesion between the different type of cells characterized by their kernels $\boldsymbol{K_i}$, the strengths a_{ij} and the shape of the force ω. On the other hand, the repulsive force due to volume constraints is modelled by a local nonlinear diffusivity depending on the total population of cells σ. The main difference with respect to the original model (Murakawa and Togashi, 2015) is the assumption that each cell counts its surrounding linearly to determine the direction of movement and the magnitude of the force decreases as the density at the cell position increases. This modification allows for a more physical balance between the total volume constraint and the adhesion forces terms. The numerical simulations in Fig. 10 were carried out in a 2D fixed domain of size $24 \times 16\sqrt{3}$ with the periodic boundary condition. The standard explicit upwind finite volume method was employed to

JNeurosci Accepted Manuscript

discretize the equations and the nonlocal terms K_i were caluculated by a numerical integral (Murakawa and Togashi, 2015; Carrillo et al., 2019). The source codes for the numerical simulations will be deposited to a public repository service.

Results

N-cadherin and phalloidin can visualize developing columns

To visualize the medulla columns, we screened a series of markers expressed in the developing fly brain. We show that the cell adhesion molecule Ncad visualizes a donut-like pattern localized at the boundary of each column in the medulla during the larval and pupal stages (Fig. 1B-D). In contrast to the single layer of this donut-like pattern in the larval brain (Fig. 1B), three layers of similar structures are found in the top (layers M1-2), middle (layers M4-5), and bottom (layers M9-10) of the medulla neuropil at 24 and 48 h after puparium formation (APF) (Fig. 1C, D). The top and middle layers derive from the distal part of the medulla neuropil early in pupal development, while the bottom layer is being formed at 24 h APF (Fig. 1C4) and is completely separated from the distal layers at 48 h APF (Fig. 1D4). The irregular arrangement of columns in the bottom layer at 24 h APF becomes well-organized by 48 h APF (Fig. 1C3, 1D3), suggesting that the columns in the bottom layer develop later than those in the top and middle layers. The clear hexagonal arrangement of the columns is observed in all three layers at 48 h APF (Fig. 1D1-3). The donut-like structure is smaller in the bottom layer than in the top and middle layers.

JNeurosci Accepted Manuscript

Additionally, the F-actin binding molecule phalloidin shows a donut-like pattern similar to that of Ncad except for the smaller hole area during the larval stage (Fig. 1B-D). Thus, Ncad and phalloidin can be used as markers to visualize the 3D structure of developing medulla columns. As demonstrated later, the arborizations of core columnar neurons overlap with these donut-like structures, suggesting that the above molecular markers precisely visualize the developing medulla columns in larval and pupal stages.

Finally, anti-Chaoptin antibody (24B10), which strongly visualizes the cell membrane of photoreceptor neurons R1-8 (Van Vactor et al., 1988), also shows a columnar donut-like pattern that overlaps with Ncad and phalloidin in third instar larvae (Fig. 1B1). However, the donut-like patterns marked by 24B10 in layers M1-2 and M4-5 are obscured at 24 h APF (Fig. 1C1-2) and are restricted to the dots inside the donuts by 48 h APF (Fig. 1D1-2). The single dots of 24B10 are localized in the peripheral parts of the columns in layers M1-2 (Fig. 1D1) or at the central position within the column in layers M4-5 at 48 h APF (Fig. 1D2).

Although synapse formation that occurs later in pupal development establishes the neural circuits within and between the columns, we only focused on the larval and early pupal stages in this study to reveal the early steps of column formation prior to synaptogenesis that have not been studied so far.

JNeurosci Accepted Manuscript

Projection patterns of essential neurons within the columns

To identify neurons that contribute to the donut-like patterns, we examined the projection patterns of neurons that project to the medulla columns: the photoreceptor neurons R7-8, the lamina neurons L1-5, and the medulla neurons Mi1 and Tm3 and lobula plate neurons T4-5 (Fischbach K.-F., 1989).

R8 is the primary neuron that induces the differentiation of other photoreceptor neurons (R1-7) in the retina (Jarman et al., 1994). Indeed, R8 axons arrive at the medulla earlier than R7 axons (Fig. 3A1-B2). Interestingly, R8 axon terminals show donut-like shapes that overlap with Ncad from mid-third instar larval stage (Figs. 2A1, 3A3). Note that the R8 terminal is not always circular but occasionally shows a horseshoe-like shape due to a gap (arrows and arrowheads in Fig. 2A1). Super-resolution imaging of the R8 terminals revealed fine filopodia emanating from the bifurcated terminals attached to each other forming a semi-circular shape (Movies 1, 2). In the following text, we call the shape of the R8 terminal "donut-like" for simplicity, except where noted otherwise. After R8, the R7 axons project to the center of the columns (Figs. 2B1, 3B). Both R8 and R7 terminate in the same layer in the larval medulla showing many filopodia, suggesting that the growth cones of R8 and R7 show the donut-like and dot-like structures, respectively (Movie 1). Note that 24B10 preferentially visualizes R8 in the larval stage, because the 24B10 signal is undetectable in the central hole area of the column where the R7 axon terminates (Figs. 1B1, 2A1-B1). These patterns gradually change during pupal development. At 48 h APF, R8 axons show semi-donut-like patterns in the superficial part of the M1 layer and faint dot-like

JNeurosci Accepted Manuscript

patterns in the middle of the column in the M3 layer (Fig. 2A2-3). The changes in the R8 terminal morphology may be due to the gradual expansion of R8 terminals from the M1 to M3 terminal layers (Ozel et al., 2015). The faint signal in the M3 layer is likely due to the immature state of the R8 growth cones and gradually becomes stronger in the later stages of pupal development (Fig. 2G). These developmental processes are regulated by multiple molecules such as Golden Goal, Flamingo (Tomasi et al., 2008; Hakeda-Suzuki et al., 2011), Ark/Jelly belly (Bazigou et al., 2007), Capricious (Shinza-Kameda et al., 2006), and Sequoia (Petrovic and Hummel, 2008; Kulkarni et al., 2016). Nevertheless, the donut-like morphology of R8 terminals has not been discussed previously. Later in this study, we will show that Ncad is essential for correct column targeting by R8.

R7 axons show strong dot-like patterns in the center of the columns in layers M4-5 (Fig. 2B3), while the dot-like pattern of R7 is faint and separate from the column center in layers M1-2 (Fig. 2B2). These results are consistent with previous observations showing that R7 axons eventually project to the M6 layer, while R8 axons initially terminate at M1 and extend to the M3 layer late in pupal development (Ting et al., 2005).

Since Gal4 drivers that are specific to each lamina neuron subtype did not show expression during larval stages, we instead used a pan-lamina Gal4 driver to visualize the axon terminals of all lamina neurons, L1-5 (Fig. 2D). We found that L1-5 axons project to the center of columns, most likely overlapping with R7 during the larval stage (Fig. 2B1, D1), but gradually expand early in pupal

JNeurosci Accepted Manuscript

development, establishing a donut-like shape overlapping with the Ncad pattern in layers M1-2 and M4-5 by 48 h APF (Fig. 2D2-3). The use of Gal4 drivers that are specific to each lamina neuron subtype suggests that the potential sources of the donut-like shape are L1 and L2 in layers M1-2 and L1 and L5 in layers M4-5 (Fig. 3G-K).

Mi1 is the primary medulla neuron that is initially produced from medulla NBs and is a unicolumnar neuron because each column contains only one Mi1 (Fischbach K.-F., 1989; Hasegawa et al., 2011). The axon terminals of Mi1 were visualized using *bshM-Gal4*, which is specifically expressed in Mi1 during the larval and early pupal stages. The Mi1 axon terminals were observed in the medulla neuropil at the early third larval instar, prior to the projections of the R8 and R7 axons (Fig. 3D). The broad pattern of Mi1 terminals is then redirected to the peripheral region outside the columns, showing a grid-like pattern surrounding the R8 terminals (Figs. 2C1, 3D, 7I). The terminals of Mi1 are found in the same layer as those of R8 and R7 in the larval medulla (Movies 1, 2). A grid-like pattern of Mi1 terminals was also observed in layers M1-2 at 48 h APF (Fig. 2C2). However, Mi1 axons partially overlap with the donut-like patterns of Ncad in layers M4-5 (Fig. 2C3). In layers M9-10, the Mi1 axon terminal forms a ring shape that clearly overlaps with the donut-like Ncad pattern (Fig. 2C4). Similar to the R8 terminal in larval medulla (Fig. 2A1), the Mi1 terminal in pupal layers M9-10 also has a gap showing a horseshoe-like shape. This is consistent with the previous observations that the Mi1 axon arborizes in layers M1, M5, and M9-10 in the pupal and adult brain (Fischbach K.-F., 1989; Hasegawa et

JNeurosci Accepted Manuscript

al., 2011). Although *bshM-Gal4* expression is also upregulated in L4 and L5 neurons during pupal development, the use of *bshL-Gal4*, which is specifically expressed in L4 and L5 throughout development, confirms that Mi1 axons are specifically visualized in the above experiments.

In contrast to Mi1, Tm3 projects to the lobula through the medulla (Fischbach K.-F., 1989; Erclik et al., 2017). Tm3 axon terminals show a grid-like pattern surrounding the columns during the larval and 48-h pupal stages, in the top, middle, and bottom layers (Fig. 2E). T4-5 are columnar lobula plate neurons that show a direction-selective response to moving visual stimuli (Maisak et al., 2013). Although T4-5 axon terminals were rarely observed in the larval medulla, they show a clear donut-like pattern in layers M9-10 at the 48 h APF pupal stage (Fig. 2F1). Since the patterns of Ncad/phalloidin staining are unidentifiable in layers M3 (between top and middle) and M6-8 (between middle and bottom) (Fig. 1D4), and the neurons examined above essentially arborize in layers M1-2, M4-5, and M9-10 (Fig. 2G), we mainly focused on these three layers in the following text, except when noted otherwise.

The above results suggest that there are three typical projection patterns of axon terminals: a dot-like pattern at the center of the column, a donut-like pattern that outlines the column, and a grid-like pattern outside the columns. During the larval stage, R7 and L1-5 show dot-like patterns, R8 shows a donut-like pattern, and Mi1 and Tm3 show grid-like patterns. During pupal development, these patterns change dynamically. At 48 h APF, R7 shows a dot-like pattern, L1-5 show donut-like patterns, and Mi1

JNeurosci Accepted Manuscript

388 shows grid-like patterns in the distal layers, while Mi1 and T4-5 show donut-like patterns in the proximal
389 layer (Fig. 2G).
390
391 **Sequential projections of the columnar neurons**
392 Among as many as 100 types of neurons in the medulla column, what are the primary core neurons
393 essential for the formation of columnar units? To address this question, we compared the timing of neural
394 projections during larval development. We found that Mi1 neurons start projecting to the medulla at the
395 mid-third instar larval stage (24-28 h L3), while R8 and R7 axons start projecting with short delays of
396 approximately 4 and 8 hours, respectively, establishing donut-like and dot-like patterns (Figs. 2, 3A-E).
397 Then, the broad projection pattern of Mi1 terminals changes to a grid-like pattern that fills the peripheral
398 region of the columns. L1-5, T4-5, and other medulla neurons project to the medulla much later in the
399 larval stage (Fig. 3C, E, F and data not shown). For example, lamina neurons project to the medulla at
400 the end of the larval stage (44-48 h L3; Fig. 3C). These results suggest that R7, R8, and Mi1 could be the
401 primary neurons for the column formation. Glial processes were not found in the developing columns in
402 larval and 48-h pupal stages (data not shown).
403
404 **R8, R7, and Mi1 are the core columnar neurons**

JNeurosci Accepted Manuscript

Next, we examined the roles of these core neurons by using mutations in which either R8, R7, or Mi1 was missing. Initially, R8 differentiation was blocked by generating *senseless* (*sens*) mutant clones (Frankfort et al., 2001). When *sens* homozygous clones were generated in the eye, loss of R8 was also revealed by the absence of R8 projection to the medulla visualized by the lack of 24B10. In our experimental condition, the clones are as large as two or three ommatidial units (Fig. 4B6). Indeed, we observed small areas as large as two or three columnar units lacking the 24B10 signal and the donut-like Ncad pattern in the larval medulla (Fig. 4B1; n=8/8) and in layers M1-2 and M4-5 in 48 h APF pupal medulla (Fig. 4B2-3; n= 9/9), suggesting that R8 is essential for medulla column formation. In layers M9-10, we also observed small areas lacking the donut-like Ncad pattern and the ring-like Mi1 axon terminals (Fig. 4A4-5, B4-5; n=4/4), suggesting that R8 influences the bottom layer to which R8 does not project. It has been reported that the *sens* mutation causes the loss of R7 (Frankfort et al., 2001). Therefore, the above defects may be indirectly caused by the loss of R7. To test this possibility, R8 was removed by expressing *reaper* (*rpr*), a potent apoptosis inducer. Since the columns were missing when R8 terminals were eliminated while R7 terminals were still present in layers M4-5, our results suggest that R8 is essential for column formation (Figs. 5A, and 1D as a control).

In the *sevenless* (*sev*) whole-body mutant in which R7 is not formed (Simon et al., 1989) , we found disorganization of columns as visualized by the donut-like Ncad pattern in the larval medulla and pupal layers M4-5 and M9-10 (Fig. 4A, C; n=14/20). The top layer (pupal layers M1-2) was not

JNeurosci Accepted Manuscript

significantly affected (Fig. 4C2). In layers M4-5 and M9-10, the donut-like column shape is not circular and there are irregular gaps between the columns (arrows in Fig. 4C3, 4). In the control, the bifurcated axon terminals of Mi1 are close to each other forming a horse shoe-like shape (Fig. 4A5). In *sev* mutant, the bifurcated axons terminals are separated and split apart (arrows in Fig. 4C5). Importantly, the abnormal columns and Mi1 axon terminals were observed in the layers to which the R7 axon does not project (Fig. 4A4-5, C4-5; n=8/12), suggesting that R7 has non-autonomous effects on column formation in the bottom layer. Since similar columnar defects were observed when *sev* was specifically knocked down in R7 (Figs. 5B, and 1D as a control), the above results confirm the important roles of R7 in the column arrangement in layers M4-5 and M9-10.

Finally, we examined the effect of the loss of Mi1 on column formation. Since *brain-specific homeobox* (*bsh*) is essential for Mi1 specification in the medulla (Hasegawa et al., 2011; Hasegawa et al., 2013), we examined *bsh* mutant brains. Strong disorganization of the shape of columns as visualized by the donut-like Ncad pattern was detected in the *bsh* whole-body mutant in the larval and three layers of the pupal medulla (Fig. 4A, D; n＝20/20). A massive disorganization of the neuropil tissue identified by the loss of Ncad signals was observed in layers M9-10 (Fig. 4A4, 4D4). These results suggest that Mi1 has important functions in organizing column formation. Since *bsh* regulates Ncad expression, Ncad expression in Mi1 and/or Mi1 projection itself may be necessary to ensure the integrity of the medulla neuropil (Hasegawa et al., 2013). Bsh is also expressed in L4 and L5 lamina neurons and is required for

JNeurosci Accepted Manuscript

441 the specification of L4 and L5 (Hasegawa et al., 2013). However, *bsh* knockdown specifically in L4-5
442 using *bshL-Gal4* caused no significant defect in column formation (data not shown), suggesting that the
443 above phenotypes were caused by the loss of *bsh* in Mi1.

444 Although L1-5-neurons project to the medulla columns much later than Mi1, R8 and R7, we have
445 examined if the ablation of L1-5 can influence the column formation in larval medulla. As expected, the
446 elimination of L1-5 by the expression of *UAS-reaper* (*rpr*) did not have a significant effect on column
447 formation (Figs. 5C, 1B, 2D1). However, it is likely that L1-5 play important roles in column formation
448 during pupal development.

449 The above results demonstrate the essential roles of R7, R8, and Mi1 as core columnar neurons in
450 the medulla, although we cannot exclude the possibility that unidentified neurons are also involved in the
451 early steps of column formation. The clearly segregated distributions of R7, R8, and Mi1 in the larval
452 columns remind us of the DAH (Steinberg, 1962). According to this hypothesis, the more-adhesive cells
453 contribute to the central part of the cell aggregates surrounded by the less-adhesive cell (Steinberg and
454 Takeichi, 1994). Similarly, the dot-like, donut-like, and grid-like patterns of R7, R8, and Mi1,
455 respectively, may reflect the order of their adhesiveness.

456

457 **Differential expression of Ncad in the core columnar neurons**

JNeurosci Accepted Manuscript

458 The mixture of cultured cells expressing different levels of cadherin has been shown to rearrange to form
459 organized cell aggregates, in which more-adhesive cells contribute to the internal part enwrapped by the
460 less-adhesive external cells (Steinberg and Takeichi, 1994). Therefore, Ncad could be a key molecule
461 that regulates column formation through its differential adhesion. Since R7, R8, and Mi1 terminals form
462 the concentric structure along the same layer in the larval medulla (Movies 1, 2), we focus on the larval
463 medulla as a model system to examine the roles of Ncad in differential adhesion and column formation.
464 As a first step to test this idea, we compared Ncad expression among the core columnar neurons R7, R8,
465 and Mi1, and in L1-5. We visualized GFP-fused Ncad in these columnar neurons by using an *Ncad*
466 knock-in allele in which endogenous *Ncad* is fused with *GFP* under the control of FLPase
467 (*Ncad-FsF-GFP*) together with FLP strains specific for columnar neurons. Ncad-GFP expression was
468 clearly detected at the terminals of R7, R8, and L1-5 (Fig. 6A, B, D). Importantly, the GFP signal was
469 detected at the center of the columns showing a dot-like pattern in larval R7 and L1-5 (Fig. 6A, D),
470 suggesting that the Ncad protein is present even within the central hole area of the columns, albeit not
471 visible via Ncad immunostaining. Intriguingly, Ncad-GFP signals were occasionally enriched at the cell
472 membrane of R7 (Fig. 6A), which might be explained by the homophilic adhesion of Ncad-GFP with
473 endogenous Ncad protein expressed in neighboring cells. Thus, the membrane accumulation of Ncad
474 could be the cause of the lack of Ncad immunostaining signal at the central hole area of the columns. We

JNeurosci Accepted Manuscript

also visualized Ncad-GFP in larval Mi1 neurons using the *homothorax* (*hth*)-*FLP* strain and anti-Bsh antibody, since Mi1 neurons are double-positive for Hth and Bsh (Fig. 6C) (Hasegawa et al., 2011).

According to the DAH, the relative levels of the cell adhesion molecules in a cell type determine the relative location of the cell within a column (Steinberg, 1962). We therefore quantified the relative expression levels of Ncad-GFP at the terminals of R7, R8, and Mi1 by using the photon counting method (Fig. 6E). In this analysis, we modified the laser power and scan speed so that the majority of pixels receive either one or two photons (Background photons were subtracted from the number of photons emitted from the axon terminals). Up to 5% pixels received three or more photons. Therefore, we assume that pixels that receive only one photon express lower levels of Ncad-GFP, while the pixels that receive two or more photons express higher Ncad-GFP levels. In contrast to the donut-like distribution of Ncad within a column, in which the Ncad signal is lower inside the central hole, the results of photon counting show that the R7 terminals located at the central hole area contain stronger Ncad-GFP signals compared with those of R8 and Mi1. For example, the percentage of pixels emitting one photon was lower for R7 compared with Mi1. In contrast, two-photon pixels were more frequent for R7 compared with R8 and Mi1. Similarly, the R8 terminals expressed Ncad-GFP more strongly than the Mi1 terminals, because there were fewer one-photon pixels and more two-photon pixels for R8 compared with Mi1. Although statistically insignificant, pixels emitting three or more photons have also shown a similar tendency in that the axon terminals contain more Ncad-GFP in the order of R7 > R8 > Mi1. Although the relative

JNeurosci Accepted Manuscript

493 densities of Ncad-GFP at the L1-5 terminals were as high as those at the R7 terminals, we cannot draw a
494 clear conclusion about the Ncad-GFP density for each subtype of L-neurons because we do not have
495 reliable subtype-specific FLP strains. Thus, the differential adhesion between R7, R8, and Mi1 can be
496 explained by differential Ncad levels among these columnar neurons.
497
498 **Roles of N-cadherin in the columnar organizations**
499 Next, we asked if Ncad-dependent differential adhesion regulates column formation. Here, we define the
500 mutant phenotype of the axon terminal as follows. Expanded: when the axon terminal shows ectopic
501 projection and resides in the original location within a column. Redirected: when the axon terminal
502 shows ectopic projections while it no longer resides in the original location within a column.
503 According to the DAH, reduction of adhesiveness would redirect the centrally located neurons
504 toward the peripheral part of the columns. Indeed, the loss of Ncad in R7 expanded its axon terminals
505 toward the peripheral part of the larval column compared with the control, in which R7 occupies the
506 central position, and the shape of the columns as visualized by Ncad and phalloidin was significantly
507 disturbed (Fig. 7A, B and data not shown). To quantify the expansion and redirection of the R7 terminals,
508 the shape of the columns needs to be preserved. Since the column morphology was largely preserved
509 when *Ncad* was knocked down in a subset of R7 by the FLP/FRT mediated clonal analysis (Fig. 7C), we
510 quantified the results in this condition. By measuring the amount of GFP signals detected within a

JNeurosci Accepted Manuscript

column or within the hole area of the column, we quantified the expansion and redirection ratios of R7, both of which were significantly larger when *Ncad* was knocked down in R7 compared with the control (Fig. 7M; see Fig. 7O and Materials and methods). Thus, the R7 terminals are expanded and redirected to the peripheral part of the columns when Ncad is reduced in R7. Similar expansion and redirection phenotypes were observed in *Ncad* loss-of-function MARCM clones (Fig. 7D; n=31/40).

The results of *Ncad* knockdown in R8 also support the roles of Ncad-dependent differential adhesion. R8 terminals were deformed and expanded to fuse with neighboring columns upon *Ncad* knockdown (Fig. 7E, F). By inducing clones of R8 in which *Ncad* was knocked down, we observed an R8 expansion phenotype (Fig. 7G). By measuring the amount of GFP signals detected within a column and within a single R8 growth cone, we quantified the expansion and redirection ratios of R8 (Fig. 7N; see Fig. 7O and Materials and methods). We found that the R8 terminals were expanded and redirected to the peripheral part of the columns when Ncad was reduced in R8. We verified the results by generating loss-of-function mutant clones of *Ncad* using the MARCM technique. As expected, the R8 terminals were expanded (Fig. 7H; n=20/20). However, we could not quantify the expansion and redirection ratios in *Ncad* mutant MARCM clones because the column morphology was completely disrupted.

According to the DAH, reduction of adhesiveness in neurons that are located at the peripheral part of the column does not significantly affect column formation. To test this idea, we knocked down

JNeurosci Accepted Manuscript

529 *Ncad* in Mi1 by using *bshMGal4*, which is specifically expressed in Mi1 during the larval stage. Loss of
530 Ncad in Mi1 showed no visible effect on column organization in the larval brain (Fig. 7 I, J). Similar
531 results were observed in *Ncad* loss-of-function MARCM clones for Mi1 (data not shown).

532 In the above experiments, we knocked down *Ncad* using two different *UAS-Ncad RNAi* strains
533 targeting distinct *Ncad* gene sequences. The effect of *Ncad* RNAi was confirmed by Ncad staining (Fig.
534 7K, L). Indeed, during pupal development, R7 terminals frequently failed to stabilize at layers M4-5
535 upon *Ncad* knockdown, which is consistent with the previous results validating the effect of RNAi (Lee
536 et al., 2001).

537 Since essentially the same results were obtained using phalloidin as a columnar marker instead
538 of Ncad and quantified in Fig. 7M, N, the above results are not due to the reduction in Ncad staining
539 induced by RNAi. These results suggest that the core columnar neurons are located within a column
540 according to differential levels of Ncad-dependent adhesion.

541 Previous extensive studies have shown the importance of Ncad for the proper targeting of R1-6 in
542 the lamina (Lee et al., 2001) as well as R7 stabilization at the M6 layer (Lee et al., 2001; Clandinin and
543 Zipursky, 2002; Ting et al., 2005; Ozel et al., 2015) and L-neuron targeting in the medulla (Nern et al.,
544 2008). However, these studies only focused on the layer targeting events in pupal stages. In this study, we
545 only focused on the earliest step of column formation in the larval stage. The mutual interactions between
546 layer targeting and column formation during pupal development will be studied in the future.

JNeurosci Accepted Manuscript

547

548 ***Ncad* knockdown reveals differential adhesion between columnar neurons**

549 According to the DAH, reduction of adhesiveness in centrally located neurons would cause a relative
550 increase in the adhesiveness of other neurons and subsequent redirection of these neurons toward the
551 central part of the columns. Since Ncad is a homophilic cell adhesion molecule, *Ncad* knockdown in one
552 cell type is expected to reduce cell adhesion with others. Therefore, we next examined the influence of
553 *Ncad* knockdown in R7 and R8 on the projection patterns of the other columnar neurons.

554 First, we examined the effects of *Ncad* knockdown in R7 on Mi1 (Fig. 8A, B). We initially
555 focused on the grid-like projection patterns of Mi1 terminals that are separated from the centrally
556 projecting R7 in larval brain. Note that there is a gap between R7 and Mi1 (arrows in Fig. 8A). Upon
557 *Ncad* knockdown, R7 terminals became diffuse and expanded. At the same time, disorganized and
558 expanded Mi1 terminals overlapped R7 (arrows and yellow signals in Fig. 8B). Since the columnar
559 morphology is significantly disrupted in this condition, we quantified the Mi1 expansion ratio by
560 measuring the Mi1 signal density within the R7 terminal area. The Mi1 expansion was significantly
561 greater when *Ncad* was knocked down in R7 (Fig. 8I). Similarly, R8 terminals were significantly
562 expanded and overlapped with R7 terminals when *Ncad* was knocked down in R7 (Fig. 8C, D, J, Movie
563 3). Although *Ncad* is thought to regulate layer targeting of R7 terminals during pupal development, we
564 found R7 terminals innervating on the larval medulla neuropil in *Ncad* RNAi conditions (Figs. 7B, C,

JNeurosci Accepted Manuscript

565 8A-D). These results are consistent with the recent finding that loss of *Ncad* causes no primary targeting
566 defects, but destabilizes R7 growth cones (Clandinin and Zipursky, 2002; Ozel et al., 2015).

567 Next, we examined the projections of Mi1 when we induced *Ncad* RNAi in R8 (Fig. 8E, F). The
568 terminals of R8 overlapping the donut-like pattern were expanded to the column periphery and fused
569 with neighboring R8 terminals in the larval brain (Fig. 8F). The filopodia of R8 were less organized
570 compared with the control. In this condition, the grid-like pattern of Mi1 was disorganized and their
571 terminals were expanded (Fig. 8F). We quantified the defect by measuring the co-localization of R8 and
572 Mi1 signals (Pearson's correlation coefficient). The overlap between R8 and Mi1 was significantly
573 greater when *Ncad* was knocked down in R8 (Fig. 8K). These results suggest that the relative
574 adhesiveness between two different cell types determines their relative location within a column.

575 When *Ncad* was knocked down in R8, R7 terminals were found enwrapped with R8 terminals,
576 and the size of the R7 terminals were 2.8 times larger compared with the control condition (Movie 4,
577 $n=32$, $p<0.001$ by *t*-test). Since R7 terminals should not be affected according to the DAH, R7 expansion
578 phenotype may be due to Ncad-independent mechanisms. As mentioned later, R7 and R8 are already
579 patterned prior to their arrival to the medulla by unknown mechanisms (see Fig. 10C). Ncad-independent
580 adhesion between R7 and R8 may be the cause of the expansion of R7 terminals as a result of R8
581 expansion.

582

JNeurosci Accepted Manuscript

Overexpression of Ncad in the columnar neurons with different levels of adhesiveness

Since the location of the neurons within the column is determined by their relative adhesiveness according to the DAH, an increase in Ncad levels in neurons that project to the peripheral part of the columns should redirect them toward the central part of the columns. To address this possibility, a *UAS-Ncad* construct that includes the entire open reading frame of *Ncad* (Iwai et al., 1997), was used to overexpress *Ncad* in the core columnar neurons Mi1, R7, and R8.

When we overexpressed *Ncad* in Mi1 neurons under the control of *bshM-Gal4*, the Mi1 terminals projecting to the grid-like domain outside the columns in the control were redirected to the column center overlapping with the donut-like Ncad and phalloidin pattern (Fig. 9A, B). The expansion and redirection ratios of Mi1 were quantified by measuring the amount of GFP signals detected within the column and the central hole area (Fig. 9I; see Fig. 7O and Materials and methods). Mi1 terminals were significantly redirected to the column center overlapping with R8 terminals. Similar results were observed when *Ncad* was overexpressed in a subset of Mi1 using the MARCM technique (Fig. 9C, D; n=11/20).

The overexpression of *Ncad* in R8 neurons led to the expansion and redirection of R8 terminals to the center of the column and the shrinkage of the central hole area (Fig. 9E, F). By measuring the amount of GFP signals detected within the hole area and a single R8 growth cone, we quantified the expansion and redirection ratios of R8 (Fig. 9J; see Fig. 7O and Materials and methods). Together with

JNeurosci Accepted Manuscript

601 the R8 expansion to the column center, R7 terminals were expanded toward the column periphery
602 overlapping with R8 terminals (Fig. 8G, H, L, Movie 5). As we expected, no significant changes were
603 observed in R7 projection after *Ncad* overexpression in R7 (Fig. 9G, H). These results are consistent
604 with the DAH and demonstrate that the core columnar neurons are located within a column according to
605 the Ncad-dependent differential adhesion.

606 The expression level of *UAS-Ncad* was confirmed by Ncad staining in the medulla neurons (Figs.
607 9K, L). The flies were cultured at 30°C to enhance the overexpression phenotype. Although we have
608 only tested a single isoform of *Ncad* (7a, 13a, 18a) for the above overexpression experiments (Iwai et al.,
609 1997), a single *Ncad* isoform has been shown to rescue the *Ncad* mutant phenotype, and the biological
610 significance of the diversity of *Ncad* isoforms has not been demonstrated (Ting et al., 2005).

611

612 **Differential adhesion of R8, R7, and Mi1 is sufficient to reproduce their columnar distributions**

613 The above results suggest that differential adhesion among R8, R7, and Mi1 plays important roles in
614 establishing their columnar distributions. However, it is unclear if differential adhesion is sufficient to
615 explain the clear segregation of the terminals of columnar neurons into three distinct domains (Fig. 10A).
616 For example, short-range repulsion between the columnar neurons may also be necessary to establish the
617 distinct domains adjacent to each other. We therefore assessed whether differential adhesion among R8,
618 R7, and Mi1 is sufficient to reproduce the wild-type and mutant patterns shown above.

JNeurosci Accepted Manuscript

The discrete cellular model is commonly used for mathematical modeling of multicellular processes. However, there are tight limitations in the size and shape of the cells in such a cell-based model. Since the terminals of columnar neurons show very irregular shapes that change dynamically, we formulated a continuous model of column formation by modifying the continuous model of cell adhesion (Murakawa and Togashi, 2015; Carrillo et al., 2019). Our model considered the densities of neurites, differential adhesion, and volume exclusion. Volume exclusion is a purely physical phenomenon distinct from active repulsion, because it only assumes that a higher cell density causes a pressure to avoid intrusion of surrounding cells. Thus, volume exclusion has an effect similar to passive repulsion. For simplicity, we only focus on R7, R8, and Mi1 during the larval stage. The valuables u, v, and w are the densities of the axon terminals of R7, R8, and Mi1, respectively (Fig. 10A). Initially, the adhesiveness of R7, R8, and Mi1 (a_{11}, a_{22}, and a_{33}) are set to 2.4, 1.8, and 0.8, respectively ($a_{11} > a_{22} > a_{33}$). The adhesiveness between two different cell types was the mean of the two different adhesiveness values ($a_{ij}=a_{ji}=(a_{ii}+a_{jj})/2$). According to their sequential projection orders, our simulations are initiated from the regularly spaced projections of R8 into the two-dimensional field uniformly covered with Mi1 terminals ($t = 0$, $v = 0.6$, $w = 0.2$; Figs. 10B1, 3A-E). Small noise is added to the initial distribution of R8. After they reach equilibrium, R7 projects in a manner identical to the initial R8 projection pattern ($t = 100$, $u = 0.6$; Fig. 10B2; yellow indicates the overlap between R7 and R8). Although there is no spatial bias between the initial distributions of R8 and R7, our model reproduces the distinct and adjacent

JNeurosci Accepted Manuscript

637 distribution patterns of R7, R8 and Mi1 showing the dot-like, donut-like, and grid-like patterns,
638 respectively, as found in larval brain (t = 1500; Figs. 2A1-C1)

639 According to the patterns of *R7-GFP* and 24B10 just below the lamina prior to the arrival at the
640 medulla in larval brain, the initial distribution patterns of R8 and R7 are actually biased (Fig. 10C). We
641 assume that the patterning of R7 and R8 occurs during the extension of their axons from the retina to the
642 medulla. R7 axons follow R8 and may be preliminarily paired with R8 by unknown mechanisms. Thus,
643 the pre-patterning of R7 and R8 should be important *in vivo*; however, the results of our mathematical
644 model in Fig. 10B show that R7 and R8 can segregate even in the absence of pre-patterning.

645 Note that 24B10 preferentially visualizes R8 in the larval stage (Figs. 1B1, 2A1). Since
646 strong 24B10 signals partially engulf R7, we repeated the numerical simulations based on the initial
647 distributions shown in Fig. 10D1. In the control, R7, R8, and Mi1 become clearly segregated, and R7 is
648 completely engulfed by R8 (t = 1000; Fig. 10D2). Qualitatively similar results are obtained by changing
649 the adhesiveness of R7, R8, and Mi1, if the order of adhesiveness is conserved ($a_{11} > a_{22} > a_{33}$; Fig.
650 10I-K), suggesting that our model reproduces the normal column formation over a wide range of
651 parameter settings. Because our model does not include any active repulsion, the results suggest that
652 differential adhesion is sufficient to explain the clear segregation of these neurons. Of course, the results
653 do not exclude the involvement of repulsive factors in column formation *in vivo*. In the presence of
654 active repulsion, columnar neurons should be segregated more robustly.

JNeurosci Accepted Manuscript

We next asked if our model also reproduces the results of our genetic experiments. When *Ncad* was knocked down in R7, R7 terminals were redirected to the peripheral region of the columns (Fig. 7A-C). Similarly, R7 terminals are expanded to the peripheral part partially engulfing R8 when the adhesiveness of R7 is reduced (a_{11} = 1.7; Fig. 10E). While R7 and Mi1 were adjacent to each other, which is consistent with Fig. 8B, R8 terminals were located outside R7 *in vivo* (Fig. 8D), most likely due to inefficient *Ncad* knock down in this condition.

Ncad knockdown in R8 caused expansion of R8 terminals and massive fusion of the columns (Fig. 7E-G). Similarly, R8 terminals are redirected to the peripheral region and fused with the neighboring columns (a_{22} = 0.6; Fig. 10F). Mi1 are redirected toward the column center, which is consistent with Fig. 8F. In contrast to the expansion of R7 terminals together with R8 *in vivo* (Movie 4), R7 terminals show a dot-like pattern separated from R8 (Fig. 10F). R7 binding with R8 may be regulated by unidentified mechanisms when *Ncad* is knocked down in R8 *in vivo*.

When *Ncad* was overexpressed in Mi1, its terminals intruded inside the columns (Fig. 9A-D). Similar phenomena were observed when the adhesiveness of Mi1 was increased (a_{33} = 1.8; Fig. 10G; magenta indicates the overlap between R8 and Mi1). Similarly to *Ncad* overexpression in R8 (Fig. 8H), an increased adhesiveness of R8 caused penetration of R8 terminals to the column center and expansion of R7 terminals toward the column periphery (a_{22} = 2.4, Fig. 10H; yellow indicates the overlap between

JNeurosci Accepted Manuscript

672 R7 and R8). Since our model only assumes basic physical properties and differential adhesiveness of the
673 cells, differential adhesion could be the major driving force to establish the columnar structure.
674
675 **Discussion**
676 **R8, R7, and Mi1 are essential core neurons for the initial step of column formation**
677 Our results suggest that the photoreceptor neurons R8 and R7 and the medulla neuron Mi1 act as core
678 neurons for the initial step of medulla column formation. At the early third instar larval stage, only Mi1
679 axons project to the medulla neuropil (Fig. 3D-E). Indeed, Mi1 is a primary medulla neuron initially
680 produced from medulla NBs (Hasegawa et al., 2011). A NB produces Drifter (Drf)-positive neurons after
681 producing Bsh-positive Mi1 neurons. However, axon terminals of Drf-positive neurons were not
682 detectable at the early third instar larval stage (Fig. 3F). At the mid-third instar stage, R8 axons and then
683 R7 axons project to the medulla (Fig 3A, B, E). The donut-like columnar patterns are then formed by the
684 end of the larval stage, as visualized by Ncad and phalloidin (Fig. 1B1).
685 Since R8 is the primary photoreceptor neuron that triggers the differentiation of other
686 photoreceptor cells (Jarman et al., 1994), R8 may also play a central role in column formation in the
687 medulla. Indeed, column formation was completely abolished in the absence of R8 axons during the
688 larval and pupal stages (Figs. 4A, B). Thus, R8 is most likely a trigger of column formation that provides
689 a spatiotemporal cue to synchronize the formation of ommatidia in the retina and columns in the medulla.

JNeurosci Accepted Manuscript

690 A similar relationship is known to exist between R axons and lamina neurons, with R axons triggering
691 the differentiation of lamina neurons (Huang and Kunes, 1996; Sato et al., 2013).

692 The column structure was also severely affected in the absence of R7 and Mi1 (Fig. 4C, D). We
693 found that the loss of R7 causes severe defects in column shape and arrangement in layers M4-5 and
694 M9-10 (Fig. 4C). The loss of Mi1 caused column distortion in layers M1-2 and M4-5 and massive
695 disorganization of the neuropil structure in layers M9-10 (Fig. 4D). These findings suggest that R8, R7,
696 and Mi1 are the essential core neurons for column formation.

697 However, projection patterns of these core neurons become diverged in the adult brain. R8 and
698 R7 axons extend and terminate in layers M3 and M6, respectively (Ting et al., 2005). Mi1 axons form
699 the bifurcated hook-like shape, which is distinct from the donut-like shape found in layers M9-10 at 48h
700 APF (Fig. 2C4) (Ke et al., 2016). Therefore, the donut-like Ncad structure found in the larval and pupal
701 stages may act as a scaffold to establish synaptic connections in the mature adult columnar structure. In
702 this study, however, we only focused on the early steps of column formation that were largely unknown.

703

704 **Differential adhesion regulates column formation**

705 Steinberg proposed the DAH to explain the self-organizing property of intermixed cells in an aggregate
706 sorting out to form an organized layered structure (Steinberg, 1962; Steinberg and Takeichi, 1994; Foty
707 and Steinberg, 2005). The idea of DAH is extensively applied in the field of synthetic biology (Toda et

JNeurosci Accepted Manuscript

al., 2018). Here, we propose that a similar strategy is used to form the columnar structure in the medulla. A similar idea has been tested in *Drosophila* lamina cartridges organized by the neurites of R1-6 and L1-5 (Schwabe et al., 2014). They demonstrated higher Ncad levels in the lamina dendrites compared with the R axons showing the concentric Ncad distribution in the lamina cartridge. A series of genetic manipulations that invert these relative differences in Ncad levels displace lamina dendrites to the periphery and R axons to the center. However, due to technical limitations, it is difficult to specifically manipulate gene activity and quantify the amount of Ncad in each of the lamina neurons, especially in the early stages. In this study, we identified the core neurons of the medulla column, R8, R7, and Mi1, and developed genetic tools to specifically quantify Ncad levels and manipulate gene activity in each of these neurons. By using these tools, we clearly demonstrated the *in vivo* evidence of DAH during columnar organization in the larval medulla.

At the beginning of column formation during larval development, R8 overlaps with the donut-like pattern of Ncad and phalloidin, while R7 shows a dot-like pattern inside the column, and Mi1 shows a grid-like pattern outside the column (Fig. 2A1-C1). We propose that the relative locations of R7, R8, and Mi1 in a layer can be explained by the DAH. Based on the dot-like, donut-like and grid-like patterns of R7, R8, and Mi1 during the larval stage, their relative adhesiveness may follow the same order, namely, R7+++, R8++, and Mi1+, respectively, because according to the DAH, the most-adhesive cells should be located in the most central position, while the least-adhesive cells surround the other cells.

JNeurosci Accepted Manuscript

The concentric domains formed by distinct and adjacent distributions of R7, R8, and Mi1 are clearly explained by our mathematical model in which only volume exclusion and differential adhesion are considered (Fig. 10), suggesting that the differential adhesion among these core neurons could play central roles in column formation. Indeed, *Ncad* knockdown in R7 and R8 expanded the projections of these neurons toward the column periphery (Fig. 7A-H, M, N). In these conditions, the R8 and Mi1 terminals expanded and overlapped with R7 (Fig. 8A-D), and the Mi1 terminals expanded and overlapped with R8 (Fig. 8E, F). On the other hand, expansion of Mi1 and R8 terminals toward the column center was detected upon overexpression of *Ncad* in these neurons (Fig. 9A-F, I, J). R7 terminals were expanded toward the column periphery when *Ncad* was overexpressed in R8 (Fig. 8G, H). Similar results were obtained by numerical simulations based on our mathematical model (Fig. 10E-H). Although L1-5 projects to the larval column center and are assumed to be the most-adhesive (Fig. 2D1), *Ncad* knockdown in L1-5 during the larval stage did not show significant defects, most likely because L1-5 project to the medulla much later than the other neurons (Fig. 3 and data not shown).

The differential adhesion of these cell types may be regulated by the differential expression levels of cell adhesion molecules such as Ncad. According to the DAH, R7 should be the most adhesive in the larval brain due to the strongest expression or activity of Ncad. Despite the lack of Ncad signals in the center of columns as visualized by Ncad staining (Fig. 2B1), the results of R7-specific Ncad-GFP visualization (Fig. 6A) and *Ncad* knockdown in R7 (Fig. 7A-C) indicate that R7 indeed produces Ncad.

JNeurosci Accepted Manuscript

744 The enrichment of Ncad-GFP at the cell membrane of R7 (arrows in Fig. 6A) or the lower density of R7
745 neurites compared with the surrounding R8 neurites may explain the loss of Ncad staining within the
746 hole. Indeed, the Ncad level was the highest in R7 among the three core columnar neurons in the larval
747 stage (Fig. 6E). Furthermore, the R8 terminals showed higher Ncad levels than the Mi1 terminals,
748 supporting the Ncad-dependent differential adhesion between R7, R8, and Mi1.

749 The behavior of R7 upon *Ncad* knock down in R8 cannot be explained solely by Ncad function
750 (Movie 4). According to the DAH, R7 should remain in the column center (Fig. 10F). However, R7
751 terminals expanded together with the R8 terminals. Ncad-independent adhesion between R7 and R8 may
752 be the cause of this phenotype.

753

754 **Inter-layer interactions between the distal and proximal layers**

755 One of the important features of column visualization by using Ncad and phalloidin is that they visualize
756 the columns in three layers of the pupal medulla. The mechanisms of three-dimensional columnar
757 organization across multiple layers would be an important issue in brain development. During the larval
758 stage, there is only one layer in the medulla column. Early in pupal development, the top and middle
759 layers are formed from the distal part of the medulla column. The bottom layers develop later than the
760 top and middle layers at 24 h APF (Fig. 1C4) and are completely separated from the distal layers at 48 h
761 APF (Fig. 1D4).

JNeurosci Accepted Manuscript

762 Our results indicate that the formation of donut-like structures in different layers is tightly
763 coupled with each other. For example, loss of R7 and R8 affected the donut-like columnar structures and
764 Mi1 axon terminals in layers M9-10, to which they do not project (Figs. 4A4-D4, 4A5-C5), suggesting
765 intimate interactions across different layers during column formation. The inter-layer interactions were
766 also observed when *Ncad* was knocked down in neurons that only project to the distal layers (data not
767 shown).

768 Numerous studies have shown that Ncad has a wide range of functions in the developing nervous
769 systems of fly and mammals (Redies et al., 1992; Redies and Takeichi, 1996; Hayashi and Carthew,
770 2004; Nern et al., 2008). Ncad is essential for the cortical organization of the mouse brain (Kadowaki et
771 al., 2007; Matsunaga et al., 2017). Therefore, Ncad-dependent differential adhesion and inter-layer
772 interaction may be the essential mechanism underlying the 3D organization of column formation that is
773 evolutionarily conserved from the fly optic lobe to mammalian brains. Future comparative studies of
774 column formation using fly and mammalian brain systems will reveal key mechanisms of columnar unit
775 formation.

776

JNeurosci Accepted Manuscript

777 **References**

778 Atkins M, Jiang Y, Sansores-Garcia L, Jusiak B, Halder G, Mardon G (2013) Dynamic rewiring of the
779 Drosophila retinal determination network switches its function from selector to differentiation.
780 PLoS genetics 9:e1003731.

781 Bazigou E, Apitz H, Johansson J, Loren CE, Hirst EM, Chen PL, Palmer RH, Salecker I (2007)
782 Anterograde Jelly belly and Alk receptor tyrosine kinase signaling mediates retinal axon
783 targeting in Drosophila. Cell 128:961-975.

784 Carrillo J A, Murakawa H, Sato M, Togashi H, Trush O (2019) A population dynamics model of cell-cell
785 adhesion incorporating population pressure and density saturation. Journal of Theoretical
786 Biology (in press).

787 Chen Y, Akin O, Nern A, Tsui CY, Pecot MY, Zipursky SL (2014) Cell-type-specific labeling of synapses
788 in vivo through synaptic tagging with recombination. Neuron 81:280-293.

789 Clandinin TR, Zipursky SL (2002) Making connections in the fly visual system. Neuron 35:827-841.

790 Erclik T, Li X, Courgeon M, Bertet C, Chen Z, Baumert R, Ng J, Koo C, Arain U, Behnia R, del Valle
791 Rodriguez A, Senderowicz L, Negre N, White KP, Desplan C (2017) Integration of temporal and
792 spatial patterning generates neural diversity. Nature 541:365-370.

793 Fischbach K.-F. DAPM (1989) The optic lobe of Drosophila melanogaster. I. A Golgi analysis of
794 wild-type structure Cell and Tissue Research 258:441-475.

JNeurosci Accepted Manuscript

795 Foty RA, Steinberg MS (2005) The differential adhesion hypothesis: a direct evaluation. Developmental
796 biology 278:255-263.
797 Frankfort BJ, Nolo R, Zhang Z, Bellen H, Mardon G (2001) senseless repression of rough is required for
798 R8 photoreceptor differentiation in the developing Drosophila eye. Neuron 32:403-414.
799 Hakeda-Suzuki S, Berger-Muller S, Tomasi T, Usui T, Horiuchi SY, Uemura T, Suzuki T (2011) Golden
800 Goal collaborates with Flamingo in conferring synaptic-layer specificity in the visual system.
801 Nature neuroscience 14:314-323.
802 Hasegawa E, Kaido M, Takayama R, Sato M (2013) Brain-specific-homeobox is required for the
803 specification of neuronal types in the Drosophila optic lobe. Developmental biology 377:90-99.
804 Hasegawa E, Kitada Y, Kaido M, Takayama R, Awasaki T, Tabata T, Sato M (2011) Concentric zones,
805 cell migration and neuronal circuits in the Drosophila visual center. Development 138:983-993.
806 Hayashi T, Carthew RW (2004) Surface mechanics mediate pattern formation in the developing retina.
807 Nature 431:647-652.
808 Huang J, Zhou W, Dong W, Watson AM, Hong Y (2009) From the Cover: Directed, efficient, and
809 versatile modifications of the Drosophila genome by genomic engineering. Proc Natl Acad Sci U
810 S A 106:8284-8289.
811 Huang Z, Kunes S (1996) Hedgehog, transmitted along retinal axons, triggers neurogenesis in the
812 developing visual centers of the Drosophila brain. Cell 86:411-422.

JNeurosci Accepted Manuscript

813 Iwai Y, Usui T, Hirano S, Steward R, Takeichi M, Uemura T (1997) Axon patterning requires
814 DN-cadherin, a novel neuronal adhesion receptor, in the Drosophila embryonic CNS. Neuron
815 19:77-89.
816 Iwai Y, Hirota Y, Ozaki K, Okano H, Takeichi M, Uemura T (2002) DN-cadherin is required for spatial
817 arrangement of nerve terminals and ultrastructural organization of synapses. Molecular and
818 cellular neurosciences 19:375-388.
819 Jarman AP, Grell EH, Ackerman L, Jan LY, Jan YN (1994) Atonal is the proneural gene for Drosophila
820 photoreceptors. Nature 369:398-400.
821 Kadowaki M, Nakamura S, Machon O, Krauss S, Radice GL, Takeichi M (2007) N-cadherin mediates
822 cortical organization in the mouse brain. Developmental biology 304:22-33.
823 Ke MT, Nakai Y, Fujimoto S, Takayama R, Yoshida S, Kitajima TS, Sato M, Imai T (2016)
824 Super-Resolution Mapping of Neuronal Circuitry With an Index-Optimized Clearing Agent. Cell
825 Rep 14:2718-2732.
826 Kondo S, Ueda R (2013) Highly improved gene targeting by germline-specific Cas9 expression in
827 Drosophila. Genetics 195:715-721.
828 Kulkarni A, Ertekin D, Lee CH, Hummel T (2016) Birth order dependent growth cone segregation
829 determines synaptic layer identity in the Drosophila visual system. Elife 5:e13715.

JNeurosci Accepted Manuscript

830 Lee CH, Herman T, Clandinin TR, Lee R, Zipursky SL (2001) N-cadherin regulates target specificity in
831 the Drosophila visual system. Neuron 30:437-450.
832 Li Y, Lu H, Cheng PL, Ge S, Xu H, Shi SH, Dan Y (2012) Clonally related visual cortical neurons show
833 similar stimulus feature selectivity. Nature 486:118-121.
834 Maisak MS, Haag J, Ammer G, Serbe E, Meier M, Leonhardt A, Schilling T, Bahl A, Rubin GM, Nern A,
835 Dickson BJ, Reiff DF, Hopp E, Borst A (2013) A directional tuning map of Drosophila
836 elementary motion detectors. Nature 500:212-216.
837 Maruoka H, Nakagawa N, Tsuruno S, Sakai S, Yoneda T, Hosoya T (2017) Lattice system of functionally
838 distinct cell types in the neocortex. Science (New York, NY) 358:610-615.
839 Matsunaga Y, Noda M, Murakawa H, Hayashi K, Nagasaka A, Inoue S, Miyata T, Miura T, Kubo KI,
840 Nakajima K (2017) Reelin transiently promotes N-cadherin-dependent neuronal adhesion during
841 mouse cortical development. Proc Natl Acad Sci U S A 114:2048-2053.
842 Morante J, Erclik T, Desplan C (2011) Cell migration in Drosophila optic lobe neurons is controlled by
843 eyeless/Pax6. Development 138:687-693.
844 Mountcastle VB (1997) The columnar organization of the neocortex. Brain : a journal of neurology 120
845 (Pt 4):701-722.
846

JNeurosci Accepted Manuscript

847 Murakawa H, Togashi H (2015) Continuous models for cell-cell adhesion. Journal of theoretical biology
848 374:1-12.
849 Neriec N, Desplan C (2016) From the Eye to the Brain: Development of the Drosophila Visual System.
850 Curr Top Dev Biol 116:247-271.
851 Nern A, Zhu Y, Zipursky SL (2008) Local N-cadherin interactions mediate distinct steps in the targeting
852 of lamina neurons. Neuron 58:34-41.
853 Noctor SC, Martinez-Cerdeno V, Ivic L, Kriegstein AR (2004) Cortical neurons arise in symmetric and
854 asymmetric division zones and migrate through specific phases. Nature neuroscience 7:136-144.
855 Ohtsuki G, Nishiyama M, Yoshida T, Murakami T, Histed M, Lois C, Ohki K (2012) Similarity of visual
856 selectivity among clonally related neurons in visual cortex. Neuron 75:65-72.
857 Ozel MN, Langen M, Hassan BA, Hiesinger PR (2015) Filopodial dynamics and growth cone
858 stabilization in Drosophila visual circuit development. Elife 4.
859 Petrovic M, Hummel T (2008) Temporal identity in axonal target layer recognition. Nature 456:800-803.
860 Pfeiffer BD, Truman JW, Rubin GM (2012) Using translational enhancers to increase transgene
861 expression in Drosophila. Proc Natl Acad Sci U S A 109:6626-6631.
862 Rakic P (1988) Specification of cerebral cortical areas. Science (New York, NY) 241:170-176.
863 Redies C, Takeichi M (1996) Cadherins in the developing central nervous system: an adhesive code for
864 segmental and functional subdivisions. Developmental biology 180:413-423.

JNeurosci Accepted Manuscript

865 Redies C, Inuzuka H, Takeichi M (1992) Restricted expression of N- and R-cadherin on neurites of the
866 developing chicken CNS. J Neurosci 12:3525-3534.
867 Rister J, Pauls D, Schnell B, Ting CY, Lee CH, Sinakevitch I, Morante J, Strausfeld NJ, Ito K,
868 Heisenberg M (2007) Dissection of the peripheral motion channel in the visual system of
869 Drosophila melanogaster. Neuron 56:155-170.
870 Sanes JR, Zipursky SL (2010) Design principles of insect and vertebrate visual systems. Neuron
871 66:15-36.
872 Sato M, Suzuki T, Nakai Y (2013) Waves of differentiation in the fly visual system. Developmental
873 biology 380:1-11.
874 Schwabe T, Borycz JA, Meinertzhagen IA, Clandinin TR (2014) Differential adhesion determines the
875 organization of synaptic fascicles in the Drosophila visual system. Current biology : CB
876 24:1304-1313.
877 Shinza-Kameda M, Takasu E, Sakurai K, Hayashi S, Nose A (2006) Regulation of layer-specific
878 targeting by reciprocal expression of a cell adhesion molecule, capricious. Neuron 49:205-213.
879 Simon MA, Bowtell DD, Rubin GM (1989) Structure and activity of the sevenless protein: a protein
880 tyrosine kinase receptor required for photoreceptor development in Drosophila. Proc Natl Acad
881 Sci U S A 86:8333-8337.

JNeurosci Accepted Manuscript

882 Steinberg MS (1962) On the mechanism of tissue reconstruction by dissociated cells. I. Population
883 kinetics, differential adhesiveness. and the absence of directed migration. Proc Natl Acad Sci U
884 S A 48:1577-1582.
885 Steinberg MS, Takeichi M (1994) Experimental specification of cell sorting, tissue spreading, and
886 specific spatial patterning by quantitative differences in cadherin expression. Proc Natl Acad Sci
887 U S A 91:206-209.
888 Takemura SY et al. (2013) A visual motion detection circuit suggested by Drosophila connectomics.
889 Nature 500:175-181.
890 Ting CY, Yonekura S, Chung P, Hsu SN, Robertson HM, Chiba A, Lee CH (2005) Drosophila
891 N-cadherin functions in the first stage of the two-stage layer-selection process of R7
892 photoreceptor afferents. Development 132:953-963.
893 Toda S, Blauch LR, Tang SKY, Morsut L, Lim WA (2018) Programming self-organizing multicellular
894 structures with synthetic cell-cell signaling. Science (New York, NY) 361:156-162.
895 Tomasi T, Hakeda-Suzuki S, Ohler S, Schleiffer A, Suzuki T (2008) The transmembrane protein Golden
896 goal regulates R8 photoreceptor axon-axon and axon-target interactions. Neuron 57:691-704.
897 Van Vactor D, Jr., Krantz DE, Reinke R, Zipursky SL (1988) Analysis of mutants in chaoptin, a
898 photoreceptor cell-specific glycoprotein in Drosophila, reveals its role in cellular morphogenesis.
899 Cell 52:281-290.

JNeurosci Accepted Manuscript

900 Yagi R, Mayer F, Basler K (2010) Refined LexA transactivators and their use in combination with the
901 Drosophila Gal4 system. Proc Natl Acad Sci U S A 107:16166-16171.
902 Yonekura S, Xu L, Ting CY, Lee CH (2007) Adhesive but not signaling activity of Drosophila
903 N-cadherin is essential for target selection of photoreceptor afferents. Developmental biology
904 304:759-770.
905 Zhu Y (2013) The Drosophila visual system: From neural circuits to behavior. Cell Adh Migr 7:333-344.
906
907

JNeurosci Accepted Manuscript

908 **Figure Legends**

909 **Figure 1. N-cadherin and phalloidin visualize developing columns.**

910 (A) Schematics of the developing larval and pupal visual systems. In the larval eye disc, R8 and R7 are
911 sequentially differentiated behind the morphogenetic furrow. The NBs, located on the surface of the
912 larval brain, produce Mi1 medulla neurons. In the pupal visual system, the retina, lamina, medulla and
913 lobula are topographically connected. Columns are identifiable along the planes indicated by dotted lines
914 in the larval and pupal brains along the three layers (top M1-2, middle M4-5 and bottom M9-10). (B-D)
915 The donut-like columnar patterns are identifiable in L3 (B1), 24h APF (C1-3) and 48h APF stages
916 (D1-3) by Ncad (green), phalloidin (blue) and 24B10 (magenta). (B1) Single layer of columnar pattern in
917 L3 larval stage. (C1-3, D1-3) Three layers of columnar patterns in 24h APF (C1-3) and 48h APF (D1-3)
918 pupal stages. Layers M1-2 (C1, D1), M4-5 (C2, D2) and M9-10 (C3, D3) are shown. Areas indicated by
919 white rectangles are shown at right (B1, C1-2, D1-2). In contrast to the clear and regular patterns in
920 layers M1-2 and M4-5 (C1-2), the columnar pattern is irregular in layers M9-10 at 24h APF (C3), which
921 become organized by 48h APF (D3). Distal to the top, dorsal to the right. The following images are
922 oriented in the same manner. (C4 and D4) Horizontal sections of 24h and 48h APF brains to visualize the
923 layers M1-2, M4-5 and M9-10. Scale bar in (B1) indicates 5um.

924

JNeurosci Accepted Manuscript

925 **Figure 2. Projection patterns of essential neurons within the columns.**

926 Projection patterns of R8, R7, Mi1, L1-5, Tm3 and T4-5 are visualized by *UAS-myrGFP* (green or white)
927 and compared with Ncad pattern (magenta). (A1-3) *sensF2-Gal4* visualizes R8 axon terminals showing
928 either donut-like (arrow) or horse shoe-like shape (arrowhead) that overlap with the donut-like Ncad
929 pattern in L3 larval stage (A1). In 48h APF pupal stage, obscured donut-like (arrows) and faint dot-like
930 patterns are identifiable in layers M1-2 (A2) and M3 (A3), respectively. (B1-3) *PM181-Gal4* visualizes
931 dot-like R7 axon terminals inside the donut-like Ncad pattern in L3 larval (B1) and 48h APF pupal
932 stages in layers M4-5 (B3). Faint dot-like patterns of R7 are also identifiable in layers M1-2 (B2). (C1-3)
933 *bshM-Gal4* visualizes grid-like Mi1 axon terminals outside the donut-like Ncad pattern in L3 larval (C1)
934 and 48h APF pupal stages in layers M1-2 (C2). Mi1 penetrates inside the donut-like Ncad pattern in
935 layers M4-5 (C3). In layers M9-10, Mi1 terminals overlap with the donut-like Ncad pattern (C4). (D1-3)
936 *R69B02-Gal4* visualizes dot-like L1-5 axon terminals inside the donut-like Ncad pattern in L3 larval
937 stage (D1). L1-5 terminals then overlap with the donut-like Ncad pattern in layers M1-2 (D2) and M4-5
938 (D3) in 48h APF pupal stage. (E1-3) *R13E12-Gal4* visualizes grid-like Tm3 axon terminals outside the
939 donut-like Ncad pattern in L3 larval (E1) and 48h APF pupal stages in layers M1-2 (E2), M4-5 (E3) and
940 M9-10 (E4). (F1) *R42F06-Gal4* visualizes T4-5 axon terminals that overlap with the donut-like Ncad
941 pattern in layers M9-10 in 48h APF pupal stage. Scale bar in (A1) indicates 5um. (G) Schematics of the
942 developing columnar units in L3 larval and 48h APF pupal stages.

JNeurosci Accepted Manuscript

Figure. 3 Sequential projections of the columnar neurons.

(A-E) Sequential projections of R8 (A), R7 (B), L1-5 (C), Mi1 (D) are visualized by *UAS-myrGFP* (white) in L3 larval stages. 24B10 (magenta) and Ncad (green). (A) R8 terminals are visualized by *sensF2-Gal4.* R8 terminals are not identifiable before 28h L3 stage (arrows in A1), start to innervate the medulla neuropil by 32h and form the donut-like pattern by 38h L3 stage (arrowheads in A2-3). (B) R7 terminals are visualized by *PM181-Gal4.* R7 terminals are not identifiable before 34h L3 stage (arrows in B1), start to innervate the medulla neuropil after 36h and form the dot-like pattern by 42h L3 stage (arrowheads in B1, B2). (C) L1-5 terminals are visualized by *R69B02-Gal4.* L1-5 terminals are not identifiable before 44h L3 stage (arrows in C1), start to innervate the medulla neuropil forming the dot-like pattern by 48h L3 stage (arrowheads in C2). Cell bodies of lamina neurons (asterisks). (D) Mi1 terminals are visualized by *bshM-Gal4.* Mi1 terminals are not identifiable before 24h L3 stage (arrows in D1), start to innervate the medulla neuropil by 28h and form the grid-like pattern by 36 h L3 stage (arrowheads in D2-4). (E) Columnar neurons project to the medulla neuropil in the order of Mi1, R8, R7 and L1-5. (F) Terminals of medulla neurons visualized by *drf-Gal4* are not identifiable in the medulla neuropil by 32h L3 stage. (G-K) Projections of individual lamina neurons are visualized by clones expressing *UAS-myrGFP* (green) in 48h APF pupal stage in layers M1-2 (G1, H1, J1, K1), M3 (I1) and

JNeurosci Accepted Manuscript

960 M4-5 (G2, J2, K2). Ncad (magenta). L1, L2, L3, L4 and L5 are visualized by clones expressing GFP
961 under the control of *c202-Gal4*, *R16H03-Gal4*, *R20A03-Gal4*, *R31C06-Gal4* and *bshL-Gal4*,
962 respectively. L1 and L2 contribute to layers M1-2, and L1 and L5 contribute to layers M4-5. (L)
963 Individual Mi1 neurons visualized by clones expressing *UAS-myrGFP* (green) are projecting to the
964 peripheral region of the columns in L3 stage. Scale bars in (A1-G1) indicate 5um.

965

966 **Figure 4. R8, R7 and Mi1 are the core columnar neurons.**

967 Columnar Ncad pattern (green), and projection patterns of R axons (24B10; magenta) and columnar
968 neurons (*UAS-myrGFP*; white) in wild type (A) and in the absence of R8 (B), R7 (C) and Mi1 (D) in L3
969 larval (A1-D1) and 48h APF pupal stages (A2-D2, layers M1-2; A3-D3, layers M4-5; A4-D4, A5-C5,
970 layers M9-10). (A) In wild type, columnar patterns of Ncad are regularly arranged. (B) In the presence of
971 *sens* mutant clones, R axon terminals of 24B10 are lost and columnar patterns of Ncad are disorganized
972 (arrows) in larval medulla (B1) and in pupal layers M1-2 (B2), M4-5 (B3) and M9-10 (B4). (B5)
973 Projection pattern of Mi1 is disorganized in layers M9-10 due to the loss of R8 in layers M1-M3. (B6)
974 *sens* mutant clone in retina is visualized by the absence of GFP (arrows). (C) In *sev* mutant brains,
975 columnar patterns of Ncad are disorganized (arrows) in larval medulla (C1) and in pupal layers M4-5
976 (C3) and M9-10 (C4). (D) In bsh^{1}/bsh^{2} brains, columnar patterns of Ncad are disorganized or fused with

JNeurosci Accepted Manuscript

977 each other (arrows) in larval medulla (D1) and in pupal layers M1-2 (D2), M4-5 (D3) and M9-10 (D4).
978 (D4) Neuropil structures visualized by Ncad are missing (arrows). (A5-C5) Regularly arranged
979 donut-like Mi1 terminals visualized by *bshM-Gal4* in layers M9-10 are partially lost in the presence of
980 *sens* mutant clones (arrows in B5) and in *sev* mutant brains (arrows in C5). Scale bar in (A) indicates
981 5um.

982

983 **Fig. 5. R8 and R7 are essential for medula column formation .**

984 (A, B) Columnar Ncad pattern (green), and projection patterns of R axons (24B10; magenta) and
985 columnar neurons (*UAS-myrGFP*; white). (A1-4) R8 is partially eliminated by expressing *rpr* under the
986 control of *sensF2-Gal4* in larval (A1) and 48h APF pupal stage (A2, layers M1-2; A3, layers M4-5; A4,
987 layers M9-10). Columnar structures are lost when R8 terminals are missing (arrows in A1-4) while R7
988 terminals are present (arrows in A3). (B1-4) R7 is partially eliminated by expressing *sevRNAi* under the
989 control of *PM181-Gal4* in larval (B1) and 48h APF pupal stage (B2, layers M1-2; B3, layers M4-5; B4,
990 layers M9-10). R axons and columnar structures are disorganized (arrows in B1, B3-4). (C) Columnar
991 Ncad pattern (green) and projection pattern of L1-5 neurons (*UAS-myrGFP*; white). L1-5 are partially
992 eliminated by expressing *rpr* under the control of *R69B02-Gal4* in larval stage. Columns are not
993 disorganized in the region where L1-5 are eliminated (arrows). Scale bar in (A1) indicates 5 um.

JNeurosci Accepted Manuscript

994

995 **Figure 6. Differential expression of N-cadherin in the columnar neurons.**

996 Ncad protein localized at the terminals of columnar neurons are visualized by combining *Ncad-FsF-GFP*
997 (green or white) and *FLPase* strains that are specific to R7 (A), R8 (B), Mi1 (C) and L1-5 (D) in L3
998 larval medulla. Ncad (magenta). (A) Ncad-GFP is visualized in R7 under the control of *R20C11-FLPG5*.
999 Note that Ncad-GFP exists in the central hole area inside the columns (arrows). (B) Ncad-GFP is
1000 visualized in R8 under the control of *sens-FLPG5*. (C) Ncad-GFP is visualized in Mi1 under the control
1001 of *hth-FLP*. Mi1 was identified by Bsh expression. (D) Ncad-GFP is visualized in L1-5 under the control
1002 of *R27G05-FLPG5* (arrows). Higher magnification images are separately visualized in the top right
1003 corner of each panel. Scale bar in (A) indicates 5um. (E) Densities of photons that derive from
1004 Ncad-GFP at the terminals of columnar neurons are compared in L3 larval brains. Histogram of photon
1005 densities at the terminals of R8, R7, Mi1, and L1-5. Percentages of pixel areas that contain one, two,
1006 three, and three to five photons are compared for each neuron type. Number of axon terminals examined:
1007 R8 (n=7), R7 (n=8), Mi1(n=6), L1-5 (n=7) . (*, ** and *** indicate $P<0.05$, 0.01 and 0.001 by *t*-test).

1008

1009 **Figure 7. Roles of N-cadherin in columnar organizations.**

JNeurosci Accepted Manuscript

Columnar Ncad pattern (green), and projection patterns of R axons (24B10; magenta) and columnar neurons (*UAS-myrGFP*; white) in wild type and *Ncad* knock-down backgrounds in L3 larval medulla. (A-D) R7 terminals visualized by *PM181-Gal4*. (A) Control. (B) *Ncad* RNAi in R7. R7 terminals are expanded and the columnar Ncad pattern is disorganized (arrows). (C) *Ncad* RNAi in a subset of R7 under the control of *R20C11-FLPG5*; *GMR>Gal80>Gal4*. R7 terminals are expanded and redirected to the column periphery (arrows) as quantified in (M). (D) *Ncad* mutant MARCM clones visualizing R7 terminals that are expanded and redirected to the periphery of the column (arrows). (E-H) R8 terminals visualized by *sensF2-Gal4*. (E) Control. (F) Ncad RNAi in R8. R8 terminals are expanded and the columnar Ncad pattern is disorganized (arrows). (G) *Ncad* RNAi in a subset of R8 under the control of *sens-FLPG5*; *GMR>Gal80>Gal4*. R8 terminals are expanded and redirected to the column periphery (arrows) as quantified in (N). (H) *Ncad* mutant MARCM clones visualizing R8 terinals that are expanded to the column periphery (arrows). Ncad staining is abolished in and around the mutant clones (arrows). (I, J) Mi1 terminals visualized by *bshM-Gal4*. (I) Control. (J) *Ncad* RNAi in Mi1. Mi1 terminals and columnar Ncad pattern are not significantly affected. Scale bar in (A) indicates 5um. (K, L) The effect of *UAS-Ncad RNAi* (BDSC27503) on Ncad protein level was tested by using *optix-Gal4 UAS-CD8GFP* (green) in larval medulla. Ncad (white). (K) Control. (L) Ncad signal is significantly down regulated in GFP-positive area indicated by white dotted lines. (M, N) Expansion and redirection ratios of R7 (M), R8 (N) are quantified according to the definition in (O). Results were statistically tested (*, ** and ***

JNeurosci Accepted Manuscript

indicate $P<0.05$, 0.01 and 0.001 by t-test). (O) *o* and *i* indicate the total GFP amount within the outer and inner rings of Ncad or phalloidin staining, respectively. *w* indicates the total GFP amount within the entire growth cone of a single R8 axon. Relative GFP density (R7 and Mi1) or amount (R8) between distinct domains was used to calculate the expansion and redirection ratios. Details are described in Materials and methods.

Figure 8. Ncad knock-down reveals differential adhesion between columnar neurons.

Influences of *Ncad* RNAi expression in columnar neurons on other neurons in L3 larval medulla. (A-D) R7 terminals are visualized by *PM181-Gal4 UAS-myrGFP* (green). (A, B) Mi1 terminals are visualized by *bshM-LexA LexAop-myrTomato* (red). (A) Control. R7 and Mi1 terminals do not overlap each other (arrows). (B) *Ncad* RNAi in R7. R7 terminals are expanded and Mi1 terminals are disorganized. R7 and Mi1 overlap each other as evident from yellow signals (arrows) as quantified in (I). (C, D) R8 terminals are visualized by *sensF2-LexA LexAop-myrTomato* (red). (C) Control. R7 terminals are enwrapped by R8 terminals (arrows). (D) *Ncad* RNAi in R7. R7 and R8 overlap each other as evident from yellow signals (arrows) as quantified in (J). (E-H) R8 terminals are visualized by *sensF2-Gal4 UAS-myrGFP* (green). (E, F) Mi1 terminals are visualized by *bshM-LexA LexAop-myrTomato* (red). (E) Control. R8 and Mi1 terminals are adjacent with each other. (F) *Ncad* RNAi in R8. R8 terminals are expanded and Mi1

JNeurosci Accepted Manuscript

terminals are disorganized (arrows). R8 and Mi1 overlap each other as quantified in (K). (G, H) R7 terminals are visualized by *sevEnS-LexA LexAop-myrTomato* (red). (G) Control. R7 terminals are enwrapped by R8 terminals. (H) *Ncad* overexpression in R8. R7 terminals are expanded toward the column center and overlap with R8 terminals as quantified in (L). Rectangles indicated by white dots are separately shown at right (A-H). Scale bars in (A) indicate 5um. (I-L) Expansion of Mi1 (I), R8 (J) and R7 terminals (L), and overlaps between R8 and Mi1 (K) are quantified and statistically tested (* and *** indicate $P<0.05$ and 0.001 by t-test).

Fig. 9 Ncad overexpression in the core columnar neurons

Columnar Ncad pattern (green), projection patterns of R axons (24B10; magenta) and columnar neurons (*UAS-myrGFP*; white) in wild type and *Ncad* overexpression backgrounds in L3 larval medulla. (A, B) Mi1 terminals visualized by *bshM-Gal4*. (A) Control. (B) *Ncad* overexpression in Mi1. Mi1 terminals are expanded toward the column center (arrows) as quantified in (I). (C, D) MARCM clones visualizing Mi1 by *bshM-Gal4 UAS-myrGFP*. (C) Control. (D) *Ncad* overexpression in a subset of Mi1 neurons visualized by GFP. Expansion of Mi1 terminals toward the center of the columns is indicated by arrows. (E, F) R8 terminals visualized by *sensF2-Gal4*. (E) Control. (F) *Ncad* overexpression in R8. R8 terminals are redirected toward the column center (arrows) and the central hole area . (G,H) R7 terminals

JNeurosci Accepted Manuscript

visualized by *PM181-Gal4*. (A) Control. (B) *Ncad* overexpression in R7. R7 terminals and columnar Ncad pattern are not significantly affected. Scale bar in (A) indicates 5um. (K, L) The effect of *UAS-Ncad* on Ncad protein level was tested by using *optix-Gal4 UAS-CD8GFP* (green) in larval medulla. Ncad (white). (K) Control. (L) Ncad signal is augmented in GFP-positive medulla neurons. (I, J) Expansion and redirection ratios of Mi1 (I), and R8 (J) are quantified according to the definition in Fig. 7O and Materials and methods.

Figure 10. The continuous mathematical model of column formation.

(A) Schematic of the configuration of a column in the control. The variables u, v and w are the densities of the terminals of R7 (green), R8 (red) and Mi1 (blue), respectively. (B) Numerical results of sequential projections of R8 (B1; t=0) and R7 (B2; t=100). Identical initial distributions of R8 and R7 produce clear concentric patterns of R7, R8 and Mi1 (B3; t=1500). (C) Segregated distribution patterns of *PM181-Gal4 UAS-myrGFP* (green) and 24B10 (red) just below the lamina prior to the arrival at the medulla, where R8 partially engulfs R7. (D-H) Results of numerical simulations based on the initial distribution pattern shown in (D1). (D1-2) Control (a_{11}=2.4, a_{22}=1.8, a_{33}=0.8). R7, R8 and Mi1 are clearly segregated (D2; t=1000). (E) R7 knock-down (a_{11}=1.7). R7 is excluded from the ring of R8 and partially enwraps R8 (t=1000). (F) R8 knock-down (a_{22}=0.6). R8 is expanded and fuses with the

JNeurosci Accepted Manuscript

neighboring columns (t=1000). (G) Mi1 overexpression (a_{33}=1.8). Mi1 penetrates the ring of R8 (t=1000). (H) R8 overexpression (a_{22}=2.4). R8 and R7 are expanded toward the column center and column periphery, respectively (t=1000). (B3, D1-2, E-H) The right panels are the three dimensional views of the results, in which z-axis indicates the density of neurites. (I-K) The adhesiveness of R7, R8 and Mi1 (a_{11}, a_{22} and a_{33}) are changed between 0.4 and 3.2 to examine the range of parameter settings by which the normal column pattern can be reproduced. (I) a_{11} is fixed to 2.4. (J) a_{22} is fixed to 1.8. (K) a_{33} is fixed to 0.8. Normal concentric columna patterns are obtained if the order of adhesiveness is conserved (yellow lines; $a_{11} > a_{22} > a_{33}$).

Movie 1. R8 and R7 project to the same layer in the larval medulla.

Superresolution image of *sensF2-LexA LexAop-myrTomato* (red) and *PM181-Gal4 UAS-myrGFP* (green) in L3 larval medulla. *sensF2-Gal4 UAS-myrGFP* (green) and *sevEnS-LexA LexAop-myrTomato* (red) show the same result.

Movie 2. R8 and Mi1 project to the same layer in the larval medulla.

JNeurosci Accepted Manuscript

Superresolution image of *sensF2-Gal4 UAS-myrGFP* (green) and *bshM-LexA LexAop-myrTomato* (red) in L3 larval medulla. *sensF2-LexA LexAop-myrTomato* (red) and *bshM-Gal4 UAS-myrGFP* (green) show the same result.

Movie 3. R7 and R8 terminals significantly overlap upon *Ncad* knockdown in R7.

Superresolution image of *Ncad* RNAi in R7. *PM181-Gal4 UAS-myrGFP* (green) and *sensF2-LexA LexAop-myrTomato* (red) in L3 larval medulla.

Movie 4. R7 terminals are expanded upon *Ncad* knockdown in R8.

Superresolution image of *Ncad* RNAi in R8. *sensF2-Gal4 UAS-myrGFP* (green) and *sevEnS-LexA LexAop-myrTomato* (red) in L3 larval medulla.

Movie 5. R8 and R7 terminals significantly overlap upon *Ncad* overexpression in R8.

Superresolution image of *Ncad* overexpression in R8. *sensF2-Gal4 UAS-myrGFP* (green) and *sev-LexA LexAop-myrTomato* (red) in L3 larval medulla.

JNeurosci Accepted Manuscript

Fig.1 N-cadherin and Phalloidin visualize developing columns

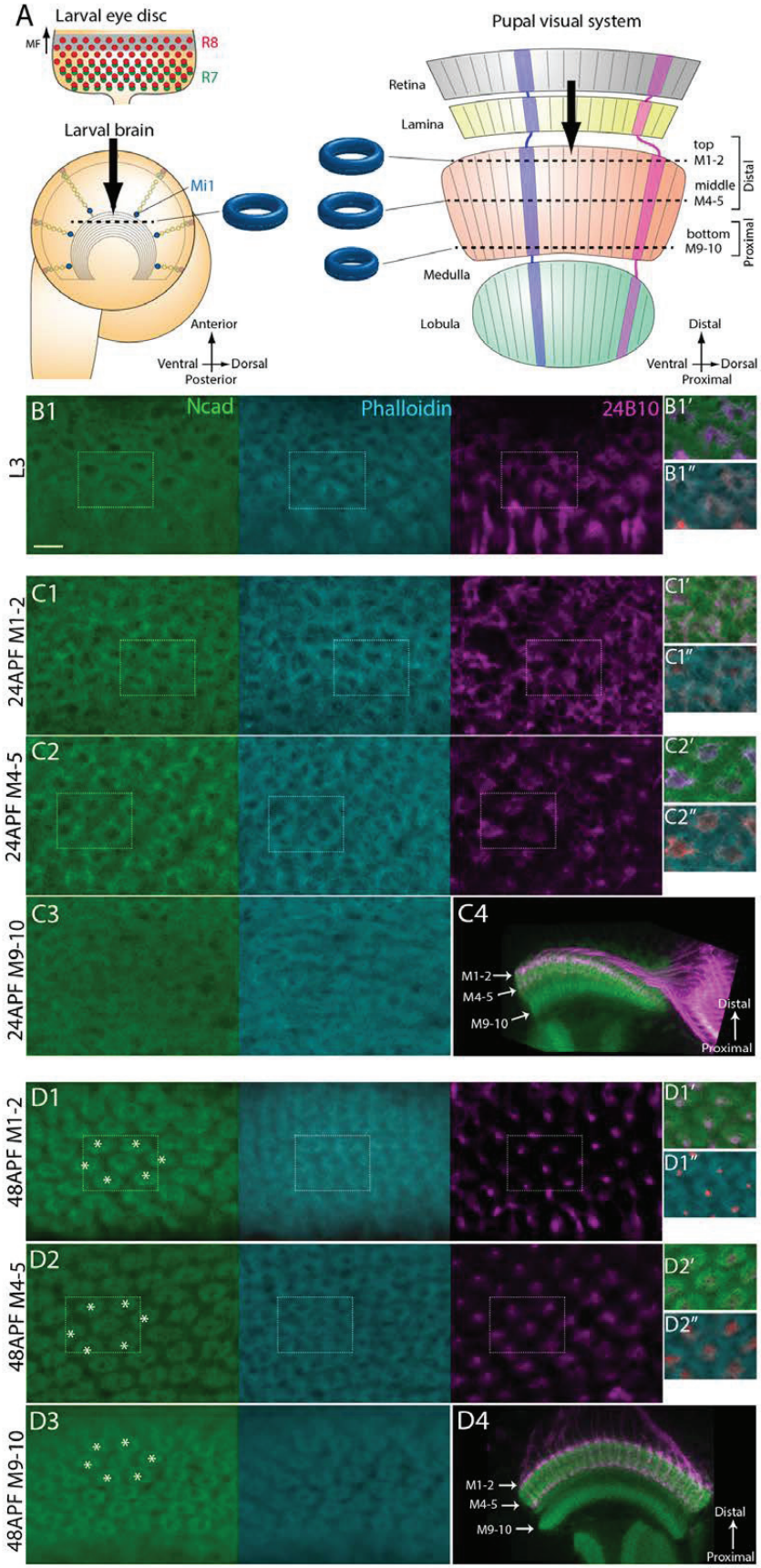

JNeurosci Accepted Manuscript

Fig. 2 Projection patterns of essential neurons within the columns

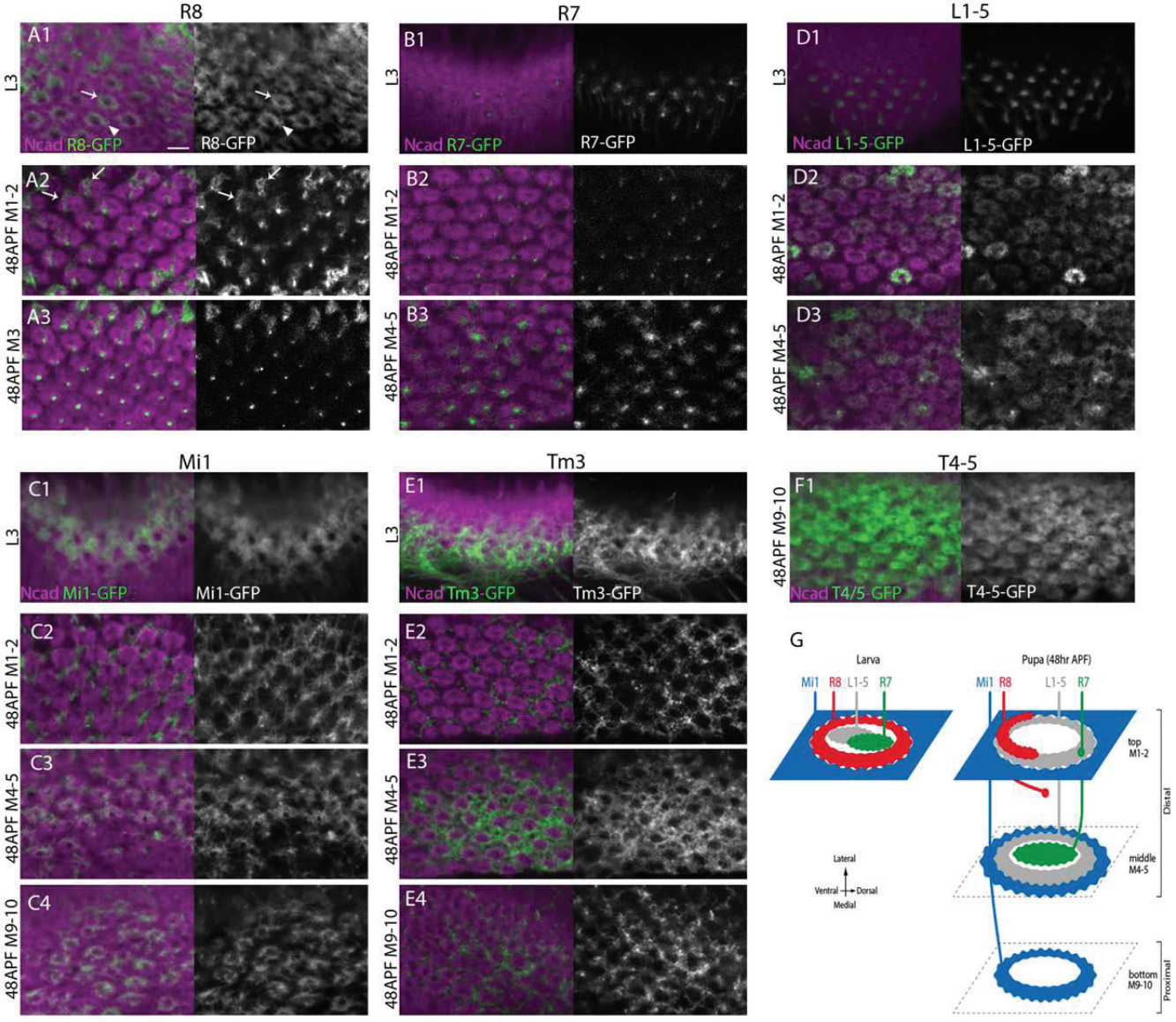

JNeurosci Accepted Manuscript

Fig. 3 Sequential projections of the columnar neurons

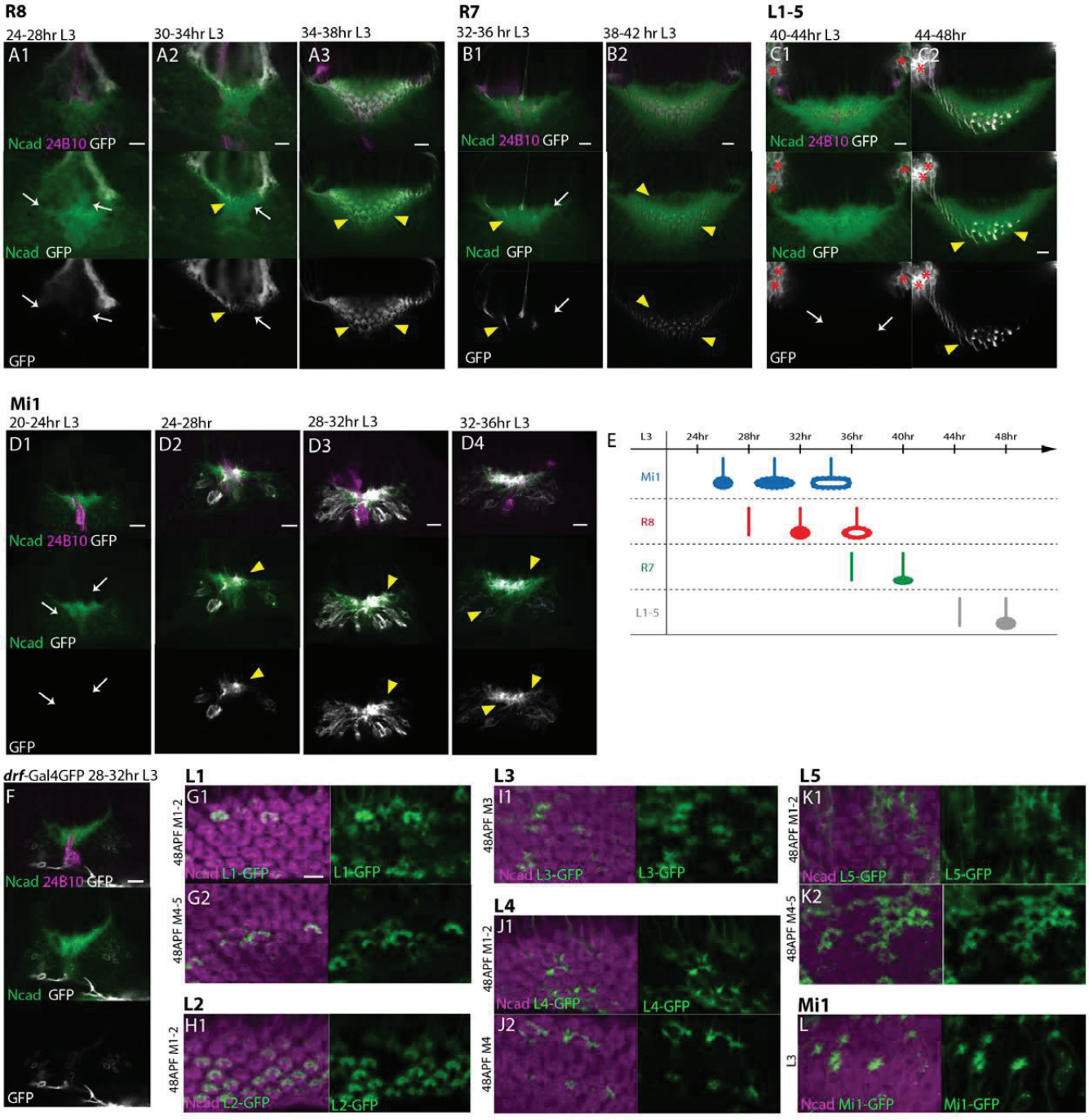

JNeurosci Accepted Manuscript

Fig 4 R8, R7 and Mi1 are the core columnar neurons

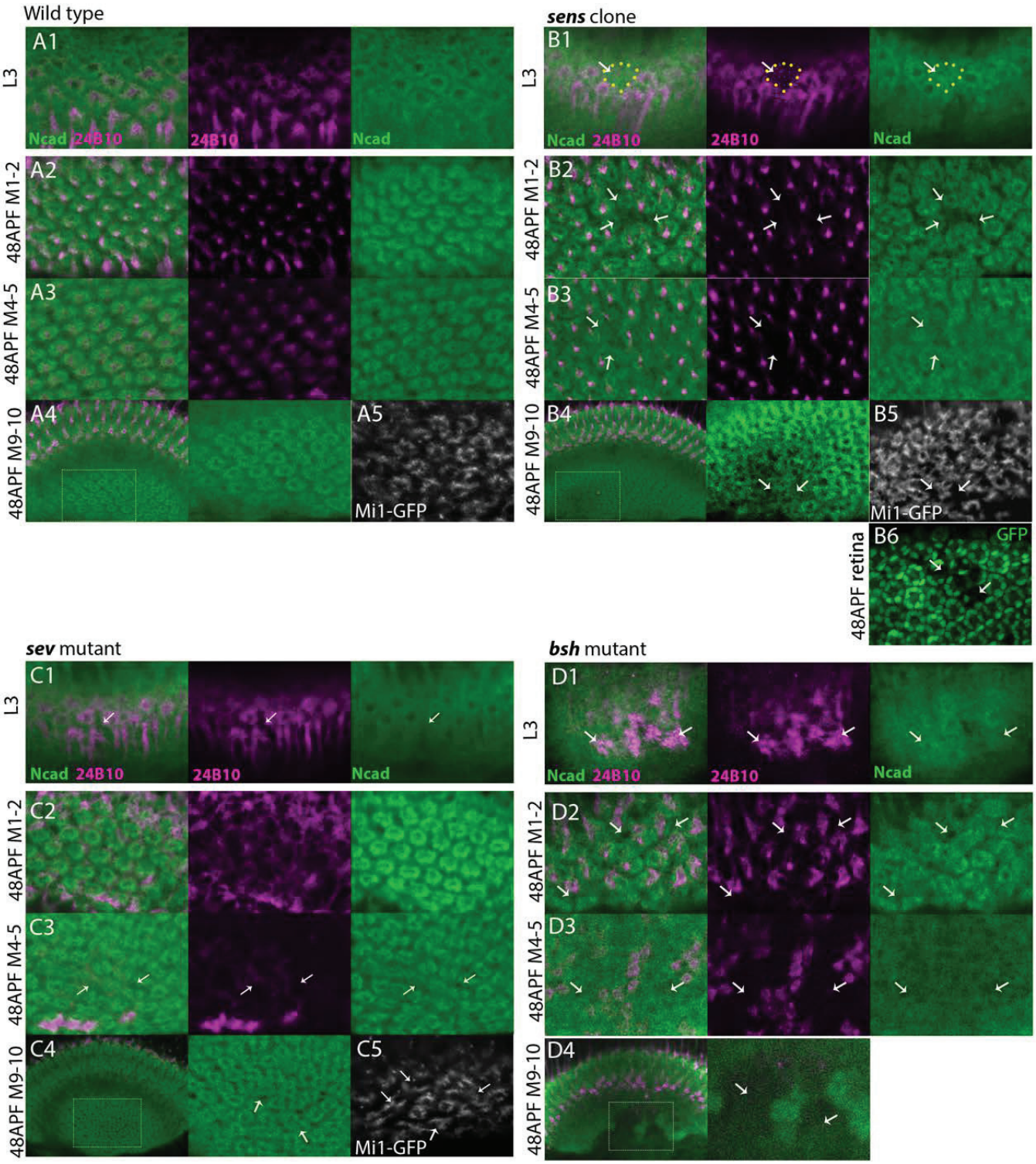

JNeurosci Accepted Manuscript

Fig. 5. R8 and R7 are essential for medulla column formation

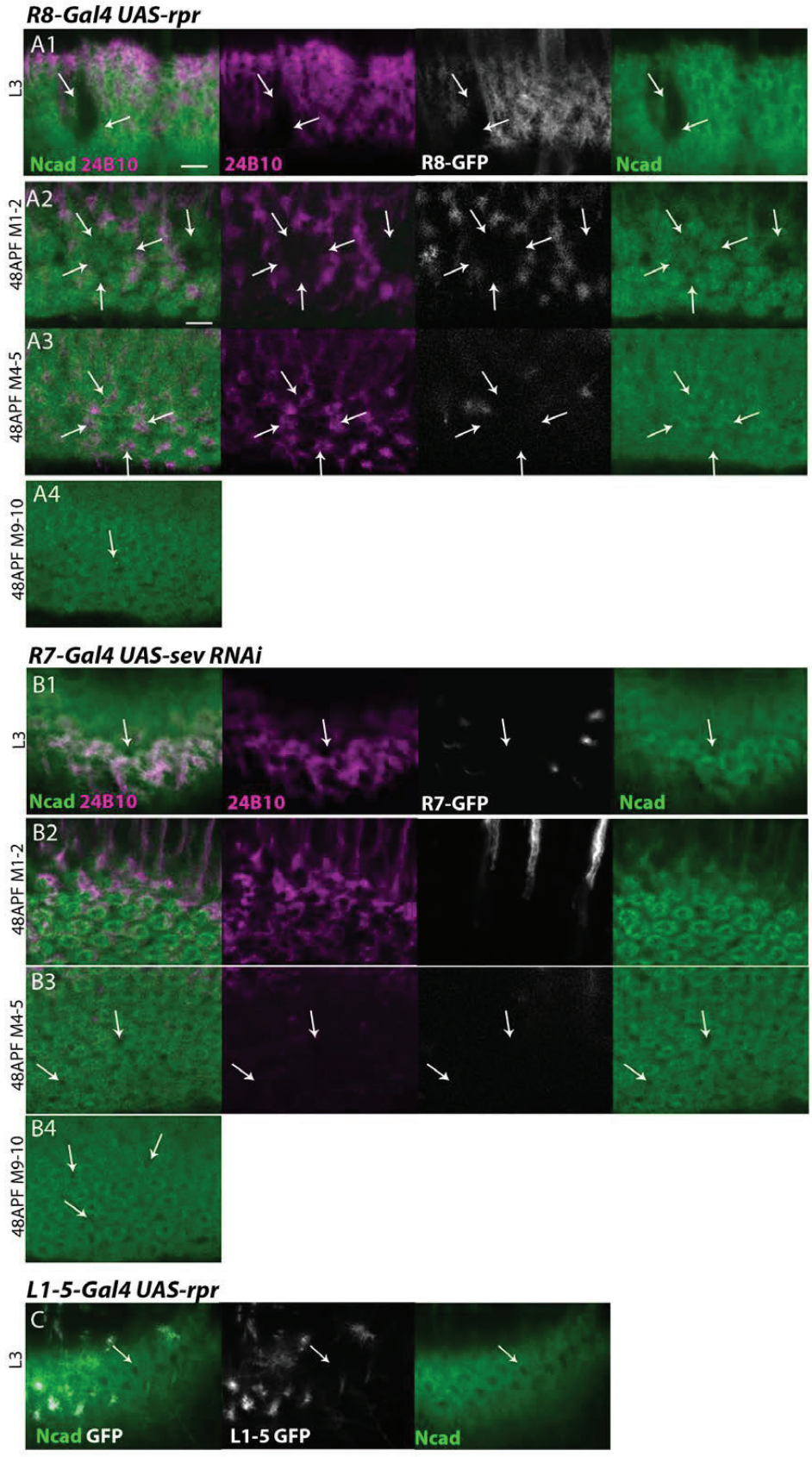

JNeurosci Accepted Manuscript

Fig. 6 Differential expression of Ncad in columnar neurons

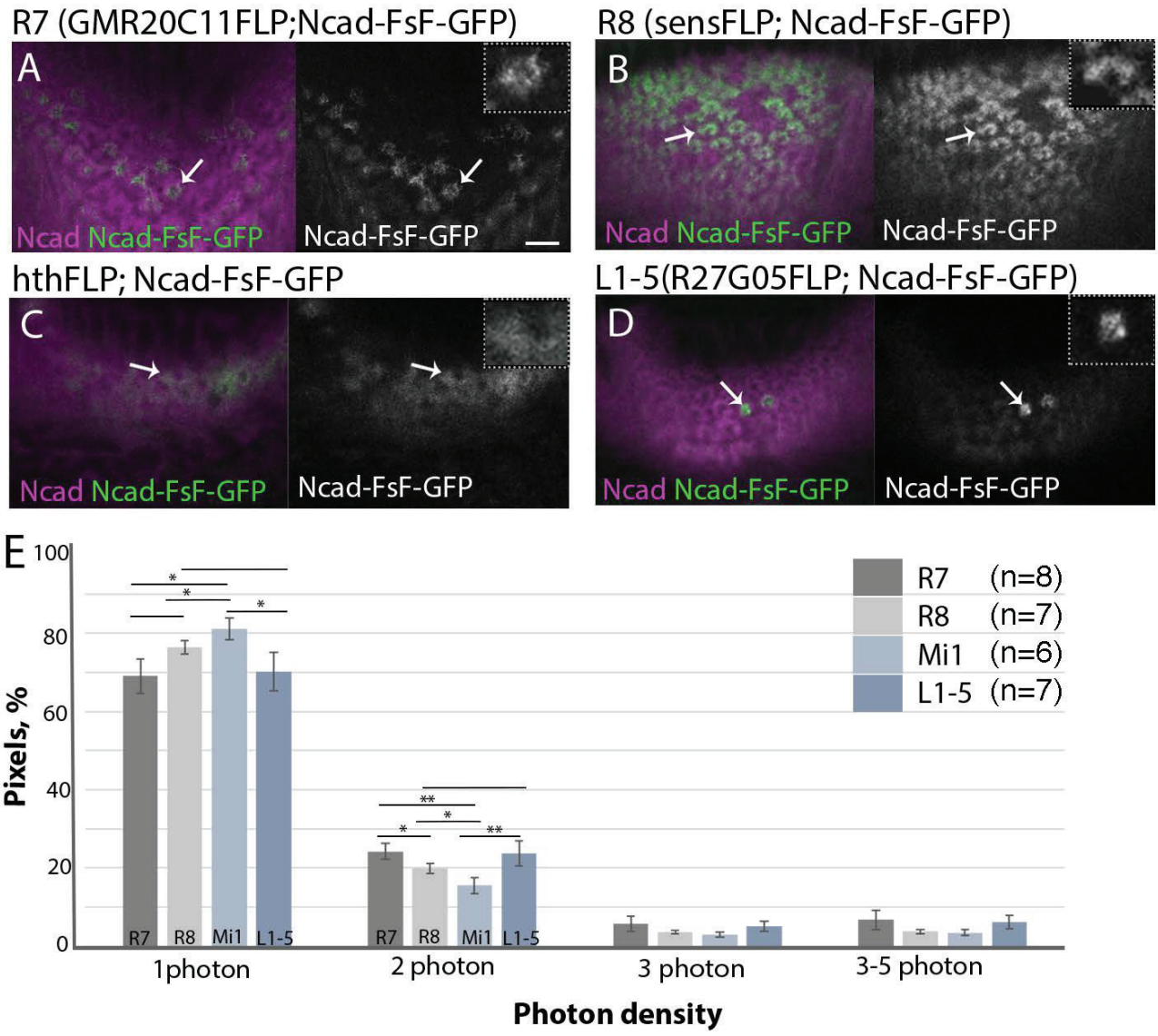

JNeurosci Accepted Manuscript

Fig. 7 Roles of N-cadherin in columnar organization

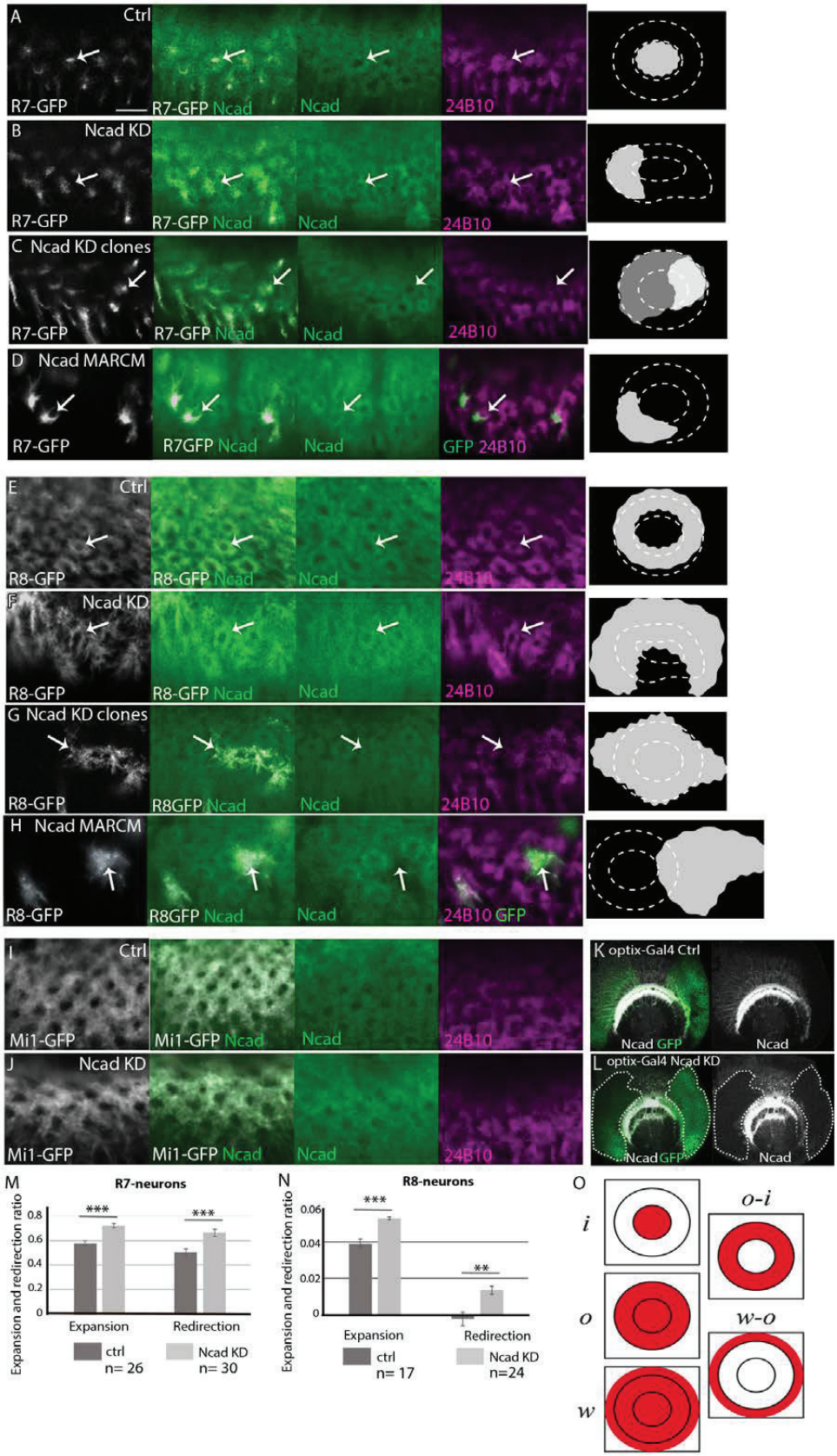

JNeurosci Accepted Manuscript

Fig. 8 Ncad knockdown reveals diferential adhesion betweencolumnar neurons

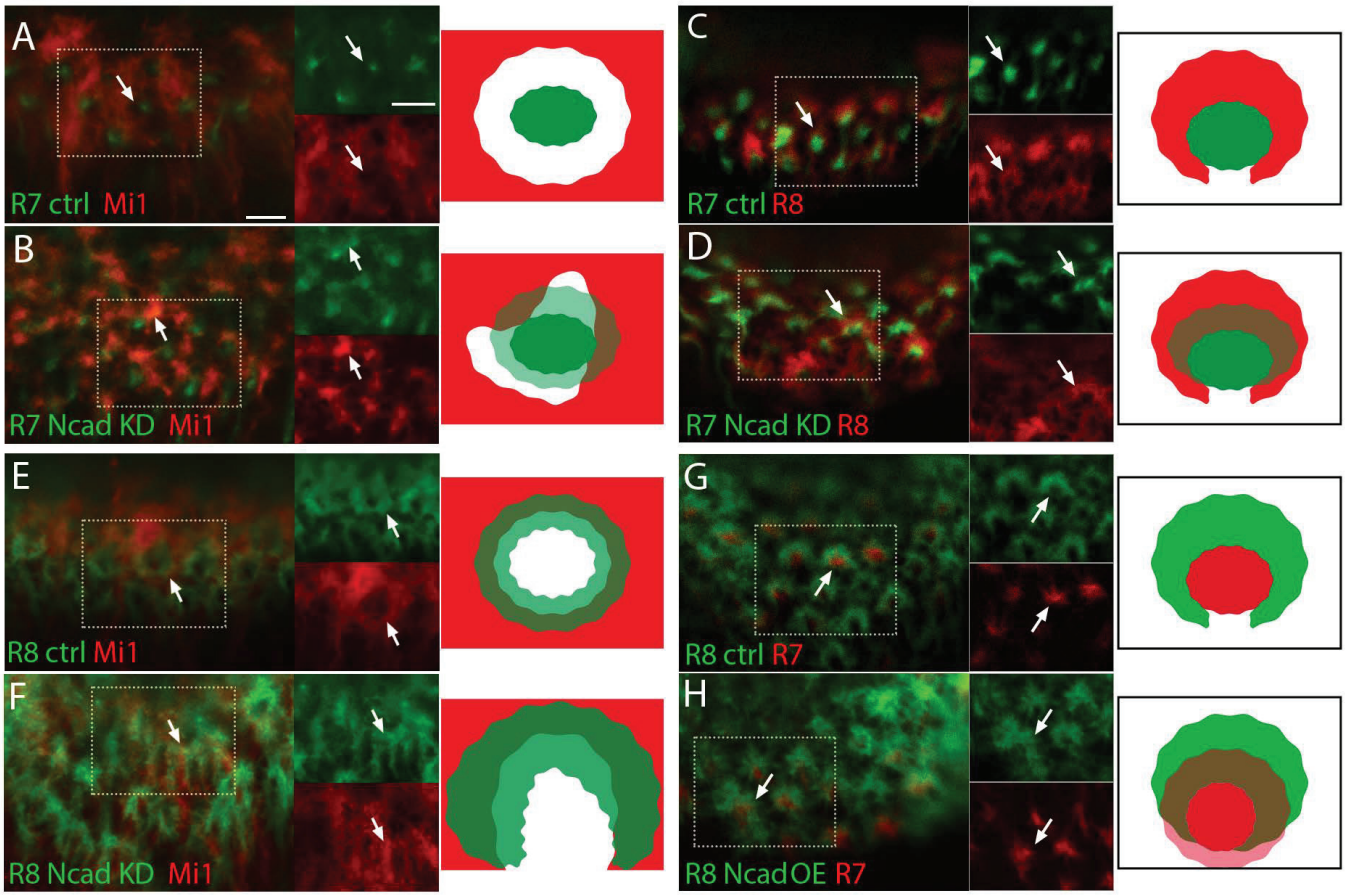

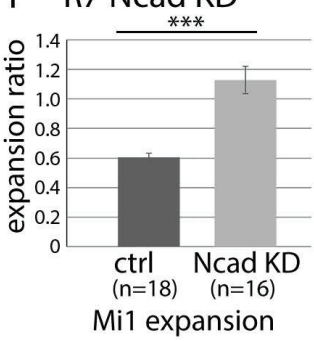

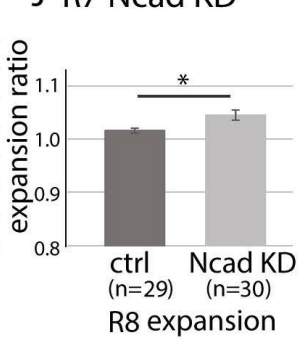

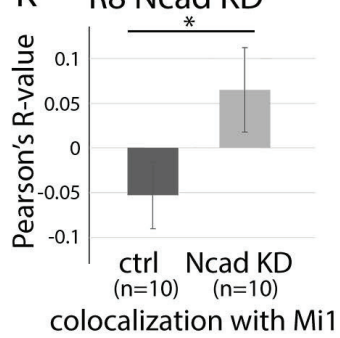

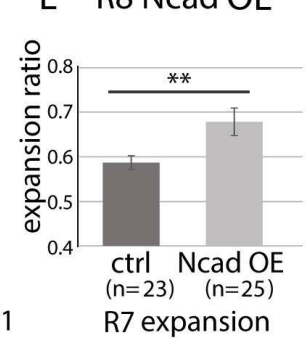

JNeurosci Accepted Manuscript

Fig. 9 Ncad overexpression in the core columnar neurons

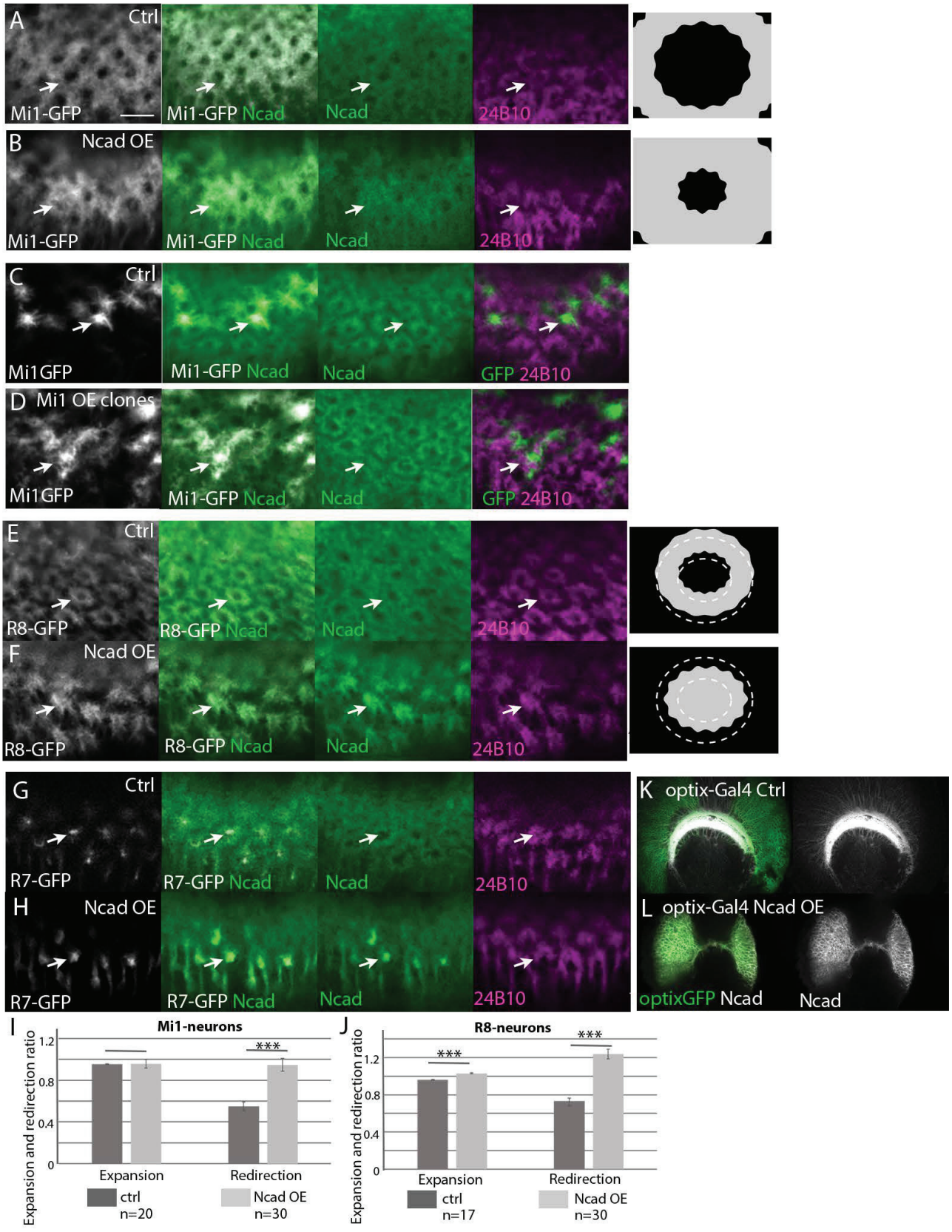

JNeurosci Accepted Manuscript
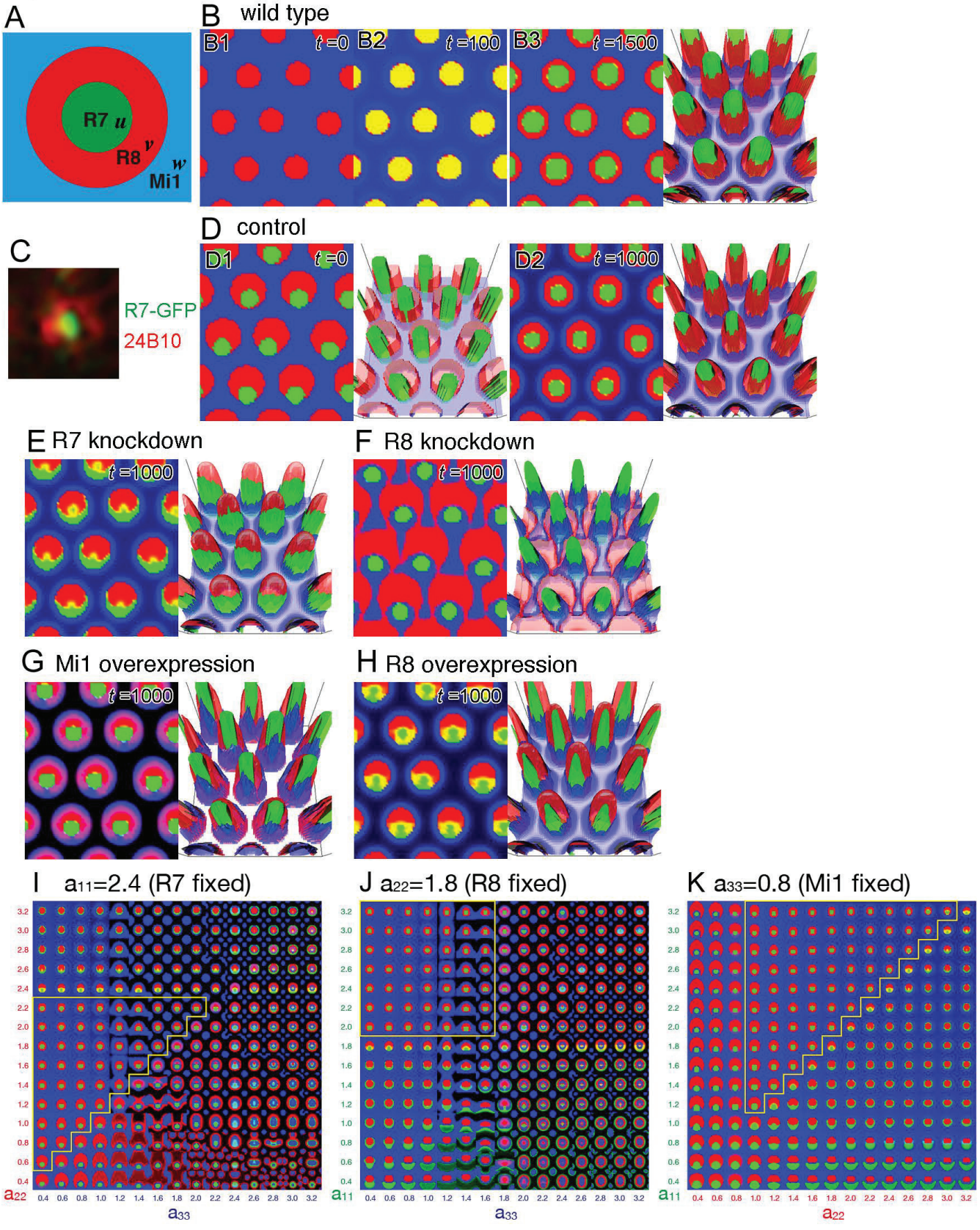
Fig. 10 The continuous mathematical model of column formation